Fernández Paz Lucía (Orcid ID: 0000-0001-5202-6809)
Echaurren Andres (Orcid ID: 0000-0001-9677-8244)
Encinas Alfonso (Orcid ID: 0000-0003-1519-1017)
Lucassen Friedrich (Orcid ID: 0000-0002-2151-6116)
Valencia Victor, A (Orcid ID: 0000-0003-2508-651X)

Constraints on trenchward arc migration and back-arc magmatism in the North Patagonian Andes in the context of Nazca plate rollback

L. Fernández Paz [1, 2], F. Bechis[3], V. D. Litvak[1, 2], A. Echaurren[1, 2], A. Encinas[4], J. González[4], F. Lucassen[5], V. Oliveros[4], V. Valencia[6], A. Folguera[1, 2]

[1] Universidad de Buenos Aires. Facultad de Ciencias Exactas y Naturales, Buenos Aires.

[2] CONICET-Universidad de Buenos Aires. Instituto de Estudios Andinos "Don Pablo Groeber" (IDEAN). Buenos Aires, Argentina.

[3] CONICET-Universidad Nacional de Río Negro, Instituto de Investigaciones en Diversidad Cultural y Procesos de Cambio (IIDyPCa), San Carlos de Bariloche, Argentina.

[4] Departamento de Ciencias de la Tierra, Universidad de Concepción, Casilla 160-C, Concepción, Chile.

[5] MARUM, Universität Bremen, D-28359; Bremen, Germany

[6] School of the Environment, Washington State University, Pullman, Washington 99164, USA.

Corresponding author: Lucía Fernández Paz (luciafp@gl.fcen.uba.ar)

Key Points:

- 33 Ma calc-alkaline volcanism (early El Maitén Belt activity) represents a mature arc front activity
- Tholeiitic early Miocene sequences (late El Maitén Belt activity) display retroarc signature with variable E-MORB-like and OIB sources
- El Maitén Belt records a magmatic evolution from a mature arc front to an extensional retroarc volcanism during Nazca plate rollback

This article has been accepted for publication and undergone full peer review but has not been through the copyediting, typesetting, pagination and proofreading process which may lead to differences between this version and the Version of Record. Please cite this article as doi: 10.1029/2019TC005580

Abstract

Geochemical and geochronological data reveal that late Oligocene-early Miocene time is a break point in the evolution of Andean magmatism. The Patagonian Andes registered the onset of arc volcanism since the late Eocene forming part of the El Maitén Belt, whose development was driven by the subduction of the Farallon/Nazca plates beneath the Andean margin. During the Oligocene, the El Maitén Belt shows a change in the geochemical signature of its magmas from tholeiitic to calc-alkaline compositions, reflecting a more mature stage in the magmatic arc evolution. Toward the early Miocene, a striking event is registered in Andean volcanic sequences as mafic tholeiitic lava flows of the El Maitén are interbedded with marine deposits, suggesting their development in the context of a fast subsiding regime. Geochemical analyses presented in this paper show that these rocks resemble E-MORB-like and OIB compositions, isotopically depleted, which strongly contrast with previous arc products. By this time, a global plate reorganization event had caused an increase in convergence rates, accelerated roll back and a more orthogonal geometry of subduction, triggering widespread magmatism and the development of extensional basins in the overriding plate. Arc-related volcanism during the early Miocene can be found only in the western slope of the Andes, suggesting the retreat of the volcanic front toward the trench. The proposed model highlights a strong linkage between the geochemical signature of magmatic products and changes in the subduction zone configuration and mantle dynamics during the evolution of the Patagonian Andes (41º–44°S).

1 Introduction

The Andes, as a 7500 km long-lived subduction-related orogen, is a perfect laboratory to test how tectonic processes left their imprint in the geochemical signature of continental arc magmas. Arc magmatism is primarily promoted by fluid-flux melting, associated with the dehydration of the subducted oceanic crust at depth, and/or decompression melting beneath the arc front (Grove et al., 2002; Huw Davies & Bickle, 1991; Pearce & Parkinson, 1993). Since the beginning of the Andean cycle, ~200 Ma ago, arc development has been conditioned by changes in the subduction zone configuration and in the crustal stress state of the margin (Cross & Pilger, 1982; DeCelles et al., 2009; Ducea et al., 2015; Lallemand et al., 2005; Lister et al., 2001; Petford et al., 1996; Schellart, 2008). Particular tectonic events often disturbed the steady state of the magmatic arc, promoting lateral variations in the position of the volcanic front and modifications in the magmatic system. These events include changes in the obliquity and dip of the subducted slab, variations in the velocity of plate convergence, subduction of oceanic floor of variable ages and collisions of mid-ocean/aseismic ridges and terrains (e.g., Aragón et al., 2013; DeCelles et al., 2009; Ducea et al., 2015; Folguera & Ramos, 2011; Kay et al., 2005; Jordan et al., 2001; Lonsdale, 2005; Ramos et al., 2014; Schellart, 2008; Somoza & Ghidella, 2012; Turner and Langmuir 2015; Turner et al. 2016).

The spatio-temporal evolution of the magmatic arc can be studied through the geochemical signature of the associated igneous rocks, as can be seen in the change from tholeiitic basalts and basaltic andesites prevalent in immature arcs, to an increasing proportion of intermediate to more silicic calc-alkaline rocks with the development of continental-type and thicker crusts (Chapman et al., 2015; Ducea et al., 2015; D'Souza et al., 2016). Besides, variations in the tectonic setting in which these magmas are created affect the composition and development of different petro-tectonic associations: crustal thickening may promote higher assimilation of preexisting crust, whereas lithospheric extension can promote the ascent of asthenospheric mantle, resulting in decompression melting and basaltic volcanism (Chapman et al., 2015; Menzies et al., 1983; D'Souza et al., 2016). Even though rarer, arc products become associated

with enriched and deeper sources, as E-MORB (Enriched Mid-Ocean Ridge Basalt) or OIB (Ocean Island Basalt) magmatism, which could reflect particular tectonic events such as backarc basin development, ridge collisions and short-lived asthenospheric anomalies (e.g., Gao et al., 2018; Kay et al., 2007, 2013).

We studied a key stage in the Cenozoic evolution of the North Patagonian Andes to evaluate how the magmatic arc developed and evolved in association with a changing tectonic framework. Late Eocene–early Miocene arc activity comprised the El Maitén Belt volcanism, located in a retroarc position compared to the previous Cretaceous arc front and recent arc activity (e.g., Echaurren et al., 2017; Fernández Paz et al. 2018; Pankhurst et al., 1999; Rapela et al., 1988). This stage was followed in the late Oligocene-early Miocene by a phase of widespread magmatism of variable signatures emplaced under extensional tectonics, thought to have temporarily interrupted Andean orogenesis and led to fore-, intra- and retro-arc basin development, in some cases associated with marine transgressions (Cazau et al., 2005; Charrier et al., 1996, 2002; Encinas et al., 2016; Jordan et al., 2001; Muñoz et al. 2000; Radic, 2010). This extensional phase took place in the framework of a global tectonic reorganization after the breakup of the Farallon plate into Nazca and Cocos plates at ~28–23 Ma, as a result of divergence of slab-pull stresses under Central America and South America subduction zones respectively (Cande & Leslie, 1986; Lonsdale, 2005; Somoza & Ghidella, 2012). This event triggered at Patagonian Andes latitudes a change from the oblique subduction of the Farallon plate to a more orthogonal subduction of the Nazca plate with increasing convergence rates (Lonsdale, 2005; Somoza & Ghidella, 2005). Basin development in relation with this extensional phase has been constrained between ~26–20 Ma (Encinas et al., 2016; Jordan et al., 2001; Muñoz et al., 2000); nevertheless, the evolution of arc-related magmatism and the geodynamic processes behind this particular setting are still matter of debate. A key point is the contrasting arc-related, E-MORB and even OIB geochemical features observed in coeval magmatic associations, which include the Coastal Magmatic Belt and the Traiguén Formation in the forearc zone, the El Maitén Belt in the retroarc zone and the Somuncura mafic plateau in the foreland (Figure 1). The most popular model to explain the magmatism of variable geochemical signatures involves a slab rollback, with a retreat of arc magmatism toward the trench and the development of forearc and backarc extensional basins (Encinas et al., 2016; Kay et al., 2007; Muñoz et al., 2000). However, open questions concerning the evolution of North Patagonian Andes by these times remain as there are no works focused on arc petrogenesis and its evolution. We explore magmatic arc evolution during protracted extension in the North Patagonian Andes, through a multidisciplinary analysis of stratigraphic, lithofacial, geochronological and geochemical/isotopic data of the El Maitén Belt. The study of two sections with different ages and compositional features provides insights into the petrogenetic response of the magmatic arc during a changing tectonic regime within a plate reorganization period.

2 Geological Setting

The studied area in the eastern North Patagonian Andes covers the northernmost sequences 41°–42°S of the El Maitén Belt (41–44°S), south of Bariloche city (Figures 1 and 2). Regionally, different north-trending morphotectonic units are from west to east the Coastal Cordillera, the Central Valley, the Main Patagonian Cordillera, and the Patagonian broken foreland (Figure 1).

The Coastal Cordillera comprises Pre-Jurassic crystalline rocks of an accretionary complex, which is partially intruded by Cretaceous to Eocene plutonic rocks (Duhart et al., 2001; Hervé et al., 2013; Thomson & Hervé, 2002; and references therein; Figure 1). These units

are covered by Cenozoic volcanic and sedimentary sequences, including Oligocene to early Miocene continental and marine deposits, which also form part of the infill of the Eocene to Quaternary basins that characterize the Central Valley (e.g., Elgueta & Mpodozis, 2012; Encinas et al., 2012, 2014; Radic et al., 2009). Volcanic units in the forearc zone include bimodal products of the Coastal Magmatic Belt and mafic volcanism of the Traiguén Formation, both of particular interest as they developed in close relationship with the mid-Cenozoic episode of widespread extension (Encinas et al., 2016; Muñoz et al., 2000; Figure 1). The Coastal Magmatic Belt is characterized by a wide lithological variability, from basalts-andesites to dacites-rhyolites, whose geochemical signature is interpreted either as transitional between arc and OIB or as arc activity developed in an extensional tectonic setting (~39–37?, 29–18.8 Ma; Henríquez Ascencio, 2016; López-Escobar & Vergara, 1997; Muñoz et al., 2000). Besides, the Traiguén Formation (~26–23 Ma) is composed of marine deposits interbedded with pillow basalts, which geochemically represent arc magmatism developed within a thinned continental crust (Encinas et al., 2016; Hervé et al., 1995; Silva, 2003).

To the east of the Central Valley, the western slope of the Main Patagonian Cordillera exposes calc-alkaline plutonic rocks of the Middle Jurassic to Miocene North Patagonian Batholith, host rock of the present Southern Volcanic Zone, whose emplacement is controlled by the dextral-transpressive Liquiñe-Ofqui Fault Zone (LOFZ) (Figure 1; Castro et al., 2011; Cembrano & Lara, 2009; Lavenu & Cembrano, 1999; López-Escobar et al., 1995; Pankhurst et al., 1999; Rolando et al., 2002; Stern, 2004). In contrast, the eastern Main Patagonian Cordillera and its foothills are structured in an east-vergent fold-thrust belt (Echaurren et al., 2017; Giacosa & Heredia, 2004; Orts et al., 2012), where Jurassic volcanic-sedimentary sequences and late Lower Cretaceous volcanic rocks with calc-alkaline affinities crop out. These units are the volcanic counterparts of the North Patagonian Batholith, which all together represent Late Jurassic to Early Cretaceous volcanic arc (Figure 1; Echaurren et al., 2017; Parada et al., 2007; and references therein).

In the retroarc zone, the Pre-Jurassic crystalline basement is exhumed over the Patagonian broken foreland (Dalla Salda et al., 1991; Pankhurst et al., 2006; Varela et al., 2015), locally intruded by Early Jurassic Subcordilleran Batholith (e.g., Rapela et al., 2005). Cenozoic sedimentary and volcanic sequences of the eastern Main Patagonian Cordillera and Patagonian broken foreland form two N- to NW- striking magmatic belts between ~40° to 43°30'S (Figure 1). The eastern Paleocene–middle Eocene Pilcaniyeu Belt (~57.8–44 Ma) includes bimodal volcanic rocks that show within-plate geochemical signatures, presumably associated with the subduction of the Aluk-Farallon mid-ocean ridge (Aragón et al., 2013; Iannelli et al., 2017). The western late Eocene–early Miocene El Maitén Belt (~37–19 Ma) includes basaltic to andesitic lava flows and subordinate dacitic to rhyolitic pyroclastic rocks with arc-related features (Figure 1; Bechis et al., 2014; Benedini et al., 2017; Fernández Paz et al., 2018; Rapela et al., 1988). It is interesting to note that the youngest volcanism of the El Maitén Belt (~23–19 Ma), found near Bariloche city (Figure 1), comprises volcanic rocks interbedded with marine deposits, forming part of the initial infill of the Ñirihuau basin (Bechis et al., 2014; Cazau et al., 2005; González Bonorino & González Bonorino, 1978; Rapela et al., 1988). A contemporaneous equivalent of the El Maitén Belt, north of Bariloche city (~39ºS), is the Aucapan Formation (~29 Ma; Ramos et al., 2014). Its volcanic rocks show an arc signature and are interpreted, together with the El Maitén Belt, as part of the late Eocene–late Oligocene arc front in a retroarc position (Iannelli et al., 2017; Rapela et al., 1988). The El Maitén Belt sequences are overlain by the Ñirihuau (~22–11 Ma) and Collón Curá (~16–10 Ma) formations, which represent the main infill of the Ñirihuau basin (Bechis

et al., 2014; Cazau et al., 1989; Ramos et al., 2015; Spalletti, 1983). While extensional conditions controlled the deposition of the basal section of the Ñirihuau Formation, its middle and upper terms and the Collón Curá Formation represent synorogenic deposits, linked to the compressional tectonic phase that affected the North Patagonian Andes at approximately ~18–11 Ma (Bechis et al., 2014, 2015; Echaurren et al., 2016; Orts et al., 2012; Ramos et al., 2015).

Further east in the foreland zone, the broad intraplate mafic volcanism of Somuncura province (~29–16 Ma) developed, partly coeval to the El Maitén Belt, being associated with a short-lived asthenospheric upwelling (de Ignacio et al., 2001; Kay et al., 2007).

3 Sampling strategy and analytical methods

The study area encompasses the northern sector of the El Maitén Belt (Figure 2a), where thick volcanic sequences crop out in Las Bayas range and in Ventana and Ñireco hills. A representative stratigraphical profile was carried out in each location to study the compositional evolution of the El Maitén Belt. Sampling strategy comprised the selection of representative lithological facies for geochemical analyses (detailed petrographic descriptions in Text S2 and S3), whose age was constrained by a new U-Pb dating in Las Bayas area, while in the Ventana-Ñireco area sampling was focused on the volcanic horizons interbedded with marine strata, with known U-Pb ages ranging from ~23 to ~19 Ma (Bechis et al., 2014). Additionally, we included a sample of the Paleozoic metamorphic basement for isotopic analyses as to evaluate crustal contamination in the studied volcanic rocks.

Geochronological analyses were done by U-Pb LA-ICPMS dating on zircons from a vitreous tuff level in the medium part of Las Bayas section. Analyses were performed out at Washington State University, using a New Wave Nd: YAG UV 213-nm laser coupled to a Thermo Finnigan Element 2 single collector, double-focusing, magnetic sector ICP-MS. Details regarding sample preparation and analysis, together with standards and results corrections, are included in Text S1 and Table S1.

Samples for geochemical analyses were prepared and analyzed at Activation Laboratories of Ancaster (Canada). Major, trace and rare earth elements were measured by total fusion and inductively coupled plasma mass spectrometry (FUS-ICP-MS). Laboratory procedures, quality controls and standards are detailed in Text S1 and Table S4.

Whole rock Sr, Nd and Pb isotope ratios were measured at Activation Laboratories Ltd. (Actlabs, Canada) and at the Center for Marine Environmental Sciences (MARUM; Bremen, Germany). Activation Laboratories performed the Sr and Nd isotopic analyses by MC-ICPMS (sample SA06) and by thermal ionization mass spectrometry (TIMS) (samples SA07 and SA08), while MARUM laboratory carried out measurements through TIMS on a Triton plus instrument (Thermo Scientific) (samples VB12b, 189, VS05, VS12 and PAT-1B). Methodologies and procedures developed during sample preparation and analyses, together with standards and normalizations, are described separately in Text S1.

4 Results: Field data, petrography and geochronology constraints on the northern El Maitén Belt

4.1 Las Bayas section

Las Bayas range is located at ~41°30’S, uplifted by a series of west-vergent backthrusts that

expose El Maitén Belt outcrops (Figure 2). The main backthrust is linked to the western slope of the range, where it uplifts a slice of the crystalline basement on its hanging wall, followed by the basal El Maitén volcanic strata (Bechis et al., 2014). The El Maitén Belt volcanism in Las Bayas range develops from the basal contact with the crystalline basement to the upper contact with the Ñirihuau Formation (Figure 2c). A secondary backthrust disturbs the volcanic sequence repeating part of its lower and middle sections. Detailed mapping allowed the complete reconstruction of the ~1320 m thick volcanic–sedimentary sequence (Figure 3a, b).

The basal part of the section corresponds to ~680 m of basaltic-andesitic to andesitic lava flows and minor volcanic breccias, tuffs, and siltstones (Figure 3b-e). Sampled andesites are porphyritic rocks with plagioclase and amphibole phenocrysts surrounded by a felty groundmass (e.g., sample 203, Figure S1). Basaltic andesites are aphanitic dark rocks that are often characterized by outcrops with columnar jointing (Figure 3d). In thin sections they show microporphyritic textures with plagioclase, clinopyroxene and orthopyroxene phenocrysts within a hyalopilitic groundmass (e.g., samples VB12b, 189 and VB07; Figure 3e). Most of the samples are fresh, though in some cases, orthopyroxenes seem pervasively altered to chlorites.

The middle part of the section (~220 m) comprise lapillitic tuffs, tuffs and minor volcanic breccias, occasionally interbedded with conglomerates and sandstones (Figure 3f). Welded tuffs with eutaxitic texture are also present with vitreous fragments molded against the lithic fragments (Figure 3g).

Finally, the upper section of the profile corresponds to ~420 m of basaltic-andesitic to andesitic lava flows, with remarkable parallel lamination and subhorizontal jointing. In some sectors, they also show a brecciated appearance. Lava flows correspond to aphyric to microporphyritic rocks, with scarce plagioclase, clinopyroxene and orthopyroxene phenocrysts (< 5 %), within a pilotaxitic groundmass (e.g., samples VB03 and SA06; Figure 3h).

Even though marine strata were not found in this section, Bechis (2004) described marine fauna in the northern sector of Las Bayas range.

The new U-Pb data of a vitreous tuff from the medium part of the section (Figure 3i) constrain volcanic activity to 33.0 ± 0.7 Ma, accordingly with the reported life-span of El Maitén Belt (upper Eocene to lower Miocene; e.g., Benedini et al., 2017; Fernández Paz et al., 2018; Rapela et al., 1988). Moreover, this lower Oligocene age lies within the range of the more frequent ages of this belt between 33–27 Ma located from 39º30’S to 42º30’S (Rapela et al., 1983, 1988). Younger ages (~22-20 Ma) are restricted to the surroundings of Bariloche city (~41–41°30’S), where the Ventana-Ñireco section crops out (Aragón, et al., 2011a; Bechis et al., 2014; González Díaz, 1979).

4.2 Ventana-Ñireco section

The Ventana and Ñireco hills are located in the northern sector of the El Maitén Belt (~41º10’S), where the thickest records of this volcanism crop out. This section comprises a ~3,500 m sedimentary and volcanic sequence, which was divided in three main members (lower, medium and upper; González Bonorino & González Bonorino, 1978). The lower and

middle members crop out at the northeastern hillslope of the Ventana hill, while the upper member lies on top of the former and continues up in the Ñireco hill (Figures 2 and 4).

Overall, the sequence is folded by NW-trending asymmetric folds with northeast vergence and uplifted over the Ñirihuau Formation by the SW-dipping Otto thrust; additionally, the sequence is overlain by the Paleozoic and Mesozoic basement rocks through the Catedral fault (Figures 2 and 4a) (Bechis et al., 2014; Giacosa et al., 2005). The age of the Ventana Formation in the Ventana-Ñireco section is constrained between ~23 and 19 Ma by U-Pb zircon ages on tuffs and sandstones of the middle and upper members (see Figures 2 and 4 for location of dated samples; Bechis et al., 2014).

The lower member consists of ~1,980 m of basaltic to andesitic lava flows and breccias, together with dacitic subvolcanic bodies. This part of the section was exempted from detailed sampling because all lava flows were moderately to intensely altered (see Text S3, Figure S2). The middle member corresponds predominantly to ~830 m of volcanic breccias with minor intercalations of lapillitic tuffs, tuffs, conglomerates and sandstones, and subordinate andesitic and basaltic lava flows. At the basal levels of this member, thick sub-vertical volcanic breccias form characteristic pinnacles, while the bedding dips are progressively gentler toward the top, closer to the syncline axis (Figure 4c). Tuffs appear as very fine-grained laminated rocks, composed mainly of crystal and vitreous fragments within a volcanic ash matrix (e.g., sample 236). Toward the uppermost part of the middle member, grayish fine-grained basalts occur, characterized by intergranular to intersertal assemblages of fresh plagioclase and clinopyroxene, with interstitial opaque minerals and devitrified glass (e.g., sample VA13).

The upper member is ~710 m thick and is composed of lapilli tuffs, tuffs and tuffaceous siltstones and sandstones, which intercalate with thick basaltic lava flows. A key feature of this upper member is the presence of interbedded marine strata that appear repeatedly within the sequence. Sampling was focused on Ñireco hill, where lava flows intercalate with marine fossiliferous wackes, tuffs and breccias (Figure 4e-f). Representative samples of these basaltic layers show microporphyritic textures either with plagioclase-clinopyroxene or olivine-plagioclase phenocryst assemblages, within intergranular to intersertal groundmasses (e.g., samples SA07, VS05, VS08 and VS12, Figure 4g). Besides, tuff levels are exposed at the top of the profile and correspond to fine-grained lithic tuffs. Volcanic lithic fragments consist of microporphyritic basaltic-andesites to aphyric basalts, while vitreous fragments include pumice and shards. Upper member tuffs were also observed in Arroyo Tristeza area (Figure 2b, sample SA03), as crystal-rich tuffs with fresh plagioclase, quartz and biotite, within a felsitic (devitrified) matrix.

A basaltic level with larger grain size and a distinctive mineralogy is interbedded within the upper section (samples SA08 and VS03; Figure 4h). It is worth to highlight that this unit crops out with a great lateral continuity all along the Ñireco hill slope (Figure 4f). It is characterized by zoned Ti-rich clinopyroxene and olivine microphenocrysts immerse within an intergranular groundmass, composed mainly of plagioclase, clinopyroxene, biotite and opaque minerals. Given its bigger grain size, its distinct petrographic features, and its concordant geometry with the sequence, it was interpreted as a sill, being unclear if it corresponds to the El Maitén Belt sequence or to a younger pulse. Despite this, it would not be much younger, as it is coherently folded with the entire sequence. Folding of these strata is related to a Miocene shortening stage, which started at between 18 and 13 Ma in the area (Bechis et al., 2014, 2015; Orts et al., 2012; Ramos et al., 2015). Therefore, the sill age is

constrained between 20 Ma, which is the maximum sedimentation age obtained for a sandstone below the sill (Figure 4b), and 13 Ma.

5 Geochemical results

Results from whole rock major and trace elements (15 samples), plus Sr, Nd and Pb isotopic ratios (6 samples) for the El Maitén Belt volcanic samples are listed in Tables S5–S8.

Studied samples of El Maitén Belt sections have variable loss-on-ignition (LOI) values, in some cases relatively high, probably implying deuteric or meteoric alteration (Tables S3 and 4). LOI contents range from 1.86 to 3.89 wt.% for samples of Las Bayas section; while samples from the Ventana-Ñireco section have values between 0.57–5.9 wt.% and the sill between 4.34–5.28 wt.%. Petrographic analyses suggest that elevated LOI contents are related mainly to Fe-Mg phyllosilicates replacing olivines and orthopyroxenes (Tables S3 and 4). Samples with LOI>5 wt.% were discarded for further analyses, as this content was associated with secondary carbonate replacements that may have caused element remobilization. Despite this, one sample of the sill with 5.28 wt.% LOI was included in the analysis, as its petrography has not shown major alteration products and the presence of primary biotite within the groundmass is thought to be a determinant factor in this elevated LOI value.

5.1 Major elements

Major element classifications show that lava flows of the Las Bayas section are andesites and dacites of subalkaline series, characterized by a restricted silica range (59.2–67.4 wt.% SiO_2; Figure 5a). Besides, K_2O (0.6–2.6 wt.%) and FeO/MgO values assign the analyzed samples to medium-K calc-alkaline series (Figures S3 and 5b).

Samples from the Ventana-Ñireco section are also subalkaline lava flows with basaltic to andesitic compositions (47.9–60.0 wt.% SiO_2), while the interbedded tuffs have rhyolitic compositions (77.7 wt.% SiO_2) (Figure 5). These samples were mostly assigned to medium-K series (0.5–1.8 wt.% K_2O), whereas FeO/MgO values differ along the section: samples from middle Ventana-Ñireco section plot in calc-alkaline fields, while samples from the upper part, mostly display tholeiitic signatures (Figure 5). Particularly, samples of the sill are characterized as alkaline tephrite-basanites (45.9–47.4 wt.% SiO_2), with high-K values (2.7–3.1 wt.% K_2O).

Despite the restricted variation in silica content, major elements of each volcanic unit (Ventana-Ñireco and Las Bayas section) display subtle trends against MgO content. General tendencies to Al_2O_3, Fe_2O_3t, MgO, CaO, TiO_2 and P_2O_5 depletion are shown against decreasing MgO content, while Na_2O and K_2O do not correlate or correlate weakly (Text S4, Figure S4).

5.2 Trace elements

Multielement diagrams show different patterns when comparing the samples from the two sections. Las Bayas section shows marked enrichment in large ion lithophile elements (LILE: Cs, Rb, Ba, Pb) with respect to high field strength elements (HFSE: Nb, Ta, P, Ti) and rare earth elements (REE: La-Lu), a typical pattern of continental arc settings. This pattern is also characterized by negative Nb-Ta, P, Ti, and positive Pb and Sr anomalies. Rare earth elements (REE) patterns are slightly concave down to relatively flat for all samples

(La/Yb=8.5–12.6; Dy/Dy*=0.52-0.63; Dy/Yb=1.51-1.81; Dy*= Dy/Dy*= $Dy_N/La_N^{4/13}\,Yb_N^{9/13}$, normalization from Nakamura, 1974), with small to insignificant Eu negative anomalies (Eu/Eu*=0.71–0.98; Eu*=(Sm+Gd)/2).

Patterns from the Ventana-Ñireco samples show variable LILE enrichment, which become less evident in samples from the upper member of the section that also lack Nb-Ta anomalies: Samples from the middle member of Ventana-Ñireco section show the highest LILE abundances, though they present lower relative contents of Rb, Ba and K in the more silicic samples. Their patterns are also characterized by Sr, P and Ti negative anomalies. Otherwise, samples from the upper member of the Ventana-Ñireco section show flat patterns akin to E-MORB series, with just small LILE enrichment respect to the HFSE and REE and minor Nb-Ta or Ti anomalies. Trace element patterns are relatively flat for all samples, with a slight concave-down curvature (La/Yb=4.0–7.1; Dy/Dy*=0.44-0.90; Dy/Yb=1.10-1.91).

In contrast to previously described basalts, subvolcanic tephrites-basanites from the analyzed sill at Ventana-Ñireco section show OIB-like patterns with enrichment in incompatible elements, Pb negative anomaly and no Nb-Ta anomalies. Furthermore, these samples show REE patterns with high slopes (La/Yb~31, Dy/Dy*=0.64–0.70; Dy/Yb=2.56–2.80).

5.3 Isotopes

Initial Sr and Nd isotope signatures of the two age groups and the sill show systematic differences, though they all largely plot with a negative correlation into the depleted mantle quadrant, within the range of the SVZ rocks (Figure 6). The Las Bayas samples are uniform with the lower $^{143}Nd/^{144}Nd_t$ (0.51264–0.51264) and highest $^{87}Sr/^{86}Sr_i$ ratio (0.7044–0.7045); whereas the Ventana-Ñireco hills samples display a wider range with lower $^{87}Sr/^{86}Sr_i$ (0.7033–0.7037) and higher $^{143}Nd/^{144}Nd_t$ (0.51281–0.51283). The sill from Ventana-Ñireco hills shows intermediate values ($^{87}Sr/^{86}Sr_i$=0.7040; $^{143}Nd/^{144}Nd_t$ =0.51272) between the signatures of Las Bayas and Ventana-Ñireco samples. Contrastingly, the Paleozoic metamorphic sample has much higher $^{87}Sr/^{86}Sr_i$ and lower $^{143}Nd/^{144}Nd_t$ values than Cenozoic samples ($^{87}Sr/^{86}Sr_i$ =0.7214; $^{143}Nd/^{144}Nd_t$ =0.5118; Figure 6).

Lead isotope ratios show minor variability within the samples of both sections, resembling typical values of the SVZ magmatic arc between orogenic and mantellic fields (Zartman and Doe, 1981; Figure 6). Las Bayas samples show relatively higher $^{207}Pb/^{204}Pb$ (15.55–15.60), $^{208}Pb/^{204}Pb$ (38.36–38.45) and $^{206}Pb/^{204}Pb$ (18.51–18.55) values than most of Ventana-Ñireco samples ($^{207}Pb/^{204}Pb$=15.52–15.60; $^{208}Pb/^{204}Pb$=38.13–38.43; $^{206}Pb/^{204}Pb$=18.48–18.52; Figure 6). It is noteworthy that the samples of the upper member of the Ventana-Ñireco section show the more primitive Pb isotopic compositions, consistent with the Sr and Nd isotopes. The sill is different and shows the lowest $^{206}Pb/^{204}Pb$ ratio (18.41) and the highest $^{208}Pb/^{204}Pb$ (38.48) and $^{207}Pb/^{204}Pb$ (15.64) ratios (Figure 6). In contrast, the sample of the Paleozoic metamorphic basement show the highest lead isotope values ($^{208}Pb/^{204}Pb$=38.96; $^{207}Pb/^{204}Pb$=15.65; $^{206}Pb/^{204}Pb$=18.80; Figure 6).

6 Discussion

6.1 Petrogenesis and magma evolution in the northern El Maitén Belt

Las Bayas (~33 Ma) section of the El Maitén Belt comprises andesites and dacites with elemental and isotopic compositions of relatively evolved rocks. Las Bayas samples are characterized by arc-like trace element patterns with marked negative Nb-Ta anomalies,

whose subparallel patterns suggest a common magma source for the whole sequence (Figure 5). As indicated by the relatively flat REE patterns and low Sm/Yb, Dy/Dy* and Dy/Yb ratios (Figure 5 and 7a), Las Bayas volcanism could be associated with melting of a depleted asthenospheric (MORB) mantle source, whose melts were modified by assimilation and/or fractional crystallization processes (e.g., Davidson et al., 2013; Pearce & Parkinson, 1993).

Variable major and trace element compositions against differentiation indexes, together with trace element patterns, point to fractionation of some mineral phases: P and Ti negative anomalies suggest apatite and Fe-Ti oxides fractionation, respectively; while concave down REE patterns, Dy/Dy* and Dy/Yb ratios indicate clinopyroxene and/or amphibole fractionation (Figures 5 and 7a; see also Figures S4 and S5, and Text S4). Small to insignificant Eu negative anomalies, together with the Sr positive ones, show scarce plagioclase fractionation (Figure 5).

Samples from Las Bayas have a relatively enriched isotopic composition and LILE-enriched trace elements patterns and ratios, which indicate significant slab-derived (fluids and sediments) and/or crustal contributions (Figures 5, 6, and 7 b, c). High Ba/Ta and La/Ta ratios of the Las Bayas samples point to fluid-induced enrichment, while Th/Yb and U/Th ratios indicate crustal or sediment contributions (Hawkesworth et al., 1997; Plank, 2005; Tatsumi & Eggins, 1995). Relatively low $^{143}Nd/^{144}Nd_t$ and high $^{87}Sr/^{86}Sr_i$ show contributions of both depleted mantle and crustal sources, but this isotopic composition is distinct from the regional basement rocks and volcanic rocks emplaced on old-thickened continental crust, which would have experienced important crustal contamination (e.g., Central Volcanic Zone, 13-28°S; Chapman et al., 2017; Ducea et al., 2015; Mamani et al., 2010; Figure 6). Instead, Las Bayas samples resemble elemental and isotopic compositions of the present SVZ, where magmas evolved through a normal to thin crust of about 35 km thick with relatively minor interaction with the crust (Hickey-Vargas et al., 2016; Jacques et al., 2013; López-Escobar et al., 1995; Stern, 2004; Figures 6 and 7). Figure 6 a and b show an assimilation and fractional crystallization model (AFC) as an attempt to estimate the amount of upper crustal assimilation necessary to explain the isotopic composition of these samples, which suggest the incorporation of 30% of Paleozoic basement in the magmas (See detail of the model in Text S5) .

Contrary to Las Bayas section, Ventana-Ñireco section has flat subparallel trace element patterns, characterized by slight LILE enrichment and subtle to absent Nb-Ta negative anomalies (Figure 5and 7c). The mafic samples (22–19 Ma) display the flattest patterns without LILE enrichment, resembling E-MORB compositions (Figure 5 e, f). In figure 7a, a model of the REE variations during mantle melting was used to identify the source of the basaltic samples and estimate its melting degree (F). The model is based on non-modal batch melting of a peridotite (Shaw, 1970) with a primitive mantle composition (McDonough and Sun, 1989). Detail of the model, mantle modes and partition coefficients are given in Text S5. Good agreement between model melts and our rocks are obtained by 5% partial melting of a spinel-bearing lherzolite mantle source.

Low LILE/HFSE ratios (low Ba/Ta, La/Ta, Th/Yb ratios) and depleted isotopic compositions (high $^{143}Nd/^{144}Nd_t$ and low $^{87}Sr/^{86}Sr_i$) reveal scarce slab and/or crustal contributions; placing samples in fields of within plate volcanic zones or backarc settings (Figures 6 and 7 b, c). Two samples show higher LILE/HFSE ratios and subtle Nb-Ta anomalies, plotting in the transition to volcanic arc setting (both have >55% SiO_2). This could indicate slight influence of the subducted slab or a remnant subduction component in the mantle wedge, which would have disappeared toward the younger pulses of the section (mafic samples). Slight differences

in the isotopic composition of the Ventana-Ñireco samples could indicate slight contributions from a crustal or an isotopically enriched source (Figure 6). Evidence of EM1 components (low $^{143}Nd/^{144}Ndi$) into the lithospheric mantle beneath Patagonia was recorded in SVZ magmas, interpreted as mantle heterogeneities derived from lower crust contributions to the mantle wedge (Turner et al. 2017).

On the other hand, the alkaline tephritic-basanitic sill intruding the uppermost levels of Ventana-Ñireco section has trace element patterns enriched in incompatible elements with high REE and no Nb-Ta anomalies, typical of subduction un-related OIB rocks (Figure 5). Trace element patterns show high slopes, with high Sm/Yb and La/Sm ratios (La/Sm=6.2; Sm/Yb=5.1; Figures 5 and 7a), more compatible with melting of a garnet-lherzolite source. Low Ba/Ta and La/Ta ratios suggest no influence of subducted components and high Ta/Yb ratios locate these samples in the Ta-enriched mantle field (Figure 7 b, c). Moreover, the isotopic composition of this unit differs with the samples of the two studied sections by its higher Pb isotopic values (Figure 6), highlighting their provenance from a different mantle source.

Overall, Th_N versus Nb_N resumes the contrasting signature of the studied magmatic sections (Th and Nb normalized to the N-MORB composition of Sun and McDonough, 1989; Figure 7d). Las Bayas samples display higher Th_N values, consistent with higher subduction contributions, typical of continental magmatic arcs; whereas, Ventana-Ñireco samples show a trend toward lower Th_N and Nb_N, reflecting minor subduction components, more akin to a backarc setting. Conversely, the sill plots in the alkaline OIB field, characterized by high Nb_N values.

Trace element ratios as proxies for crustal thickness are based on the concept that the evolution of arc magmas, melting and magmatic differentiation, occur at deeper average levels on a thicker crust than those developed on thinner ones. In this line, we apply different proxies regarding silica content, Ce/Y for basic rocks (Mantle & Collins, 2008) and $(La/Yb)_N$ and Sr/Y for intermediate rocks (Chapman et al., 2015; Chiaradia, 2015; Profeta et al., 2015), obtaining a clear correlation and a marked difference between the two sections. Las Bayas samples show higher $(La/Yb)_N$ and Sr/Y than Ventana-Ñireco samples, which implies a higher average depth at which magmatic fractionation would have occurred (Figure 7f-h). Very low Ce/Y, $(La/Yb)_N$ and Sr/Y values of Ventana-Ñireco samples suggest that magmatic differentiation occurred within a thinned crust.

6.2 Tectonic evolutionary model

6.2.1 Late Eocene-early Oligocene: Arc establishment

Before the development of the El Maitén Belt magmatism in the North Patagonian Andes, Paleocene-middle Eocene time was characterized by the subduction of the Aluk plate beneath the South American plate, while the Aluk-Farallon mid-ocean ridge migrated southward along the margin (Cande & Leslie, 1986; Somoza & Ghidella, 2005, 2012). Recent plate reconstructions show low absolute convergence rates for this period that could have led to extensional conditions along the margin, which went along with the development of the intraplate associations of the Pilcaniyeu Belt in the former backarc and a waning in arc activity as the subducted plate decelerated (Figures 7 and 8 a, b; ~57.8–44 Ma; Aragón et al., 2011b, 2013; Iannelli et al., 2017; Matthews et al., 2016; Somoza & Ghidella, 2005). Aragón et al. (2011b, 2013) proposed that after the subduction of the Aluk-Farallon mid-ocean ridge, the Aluk plate detached and the subduction of the Farallon plate was interrupted. Recent

studies focused both in the Andean margin as well as in other subduction zones around the world had shown that after ridge subduction, a period of slow subduction occurred until slab pull force was restored and so, arc magmatism (Fennell et al., 2018; Sun et al., 2018).

Arc activity resumed at North Patagonian latitudes by late Eocene times, forming part of the earliest products of the El Maitén Belt (~37 Ma; Fernández Paz et al., 2018). This initial magmatism consisted of tholeiitic lava flows, generated mainly by decompression melting with subordinate slab contributions, which would have been emplaced within the context of an extensional regime (Echaurren et al., 2016; Fernández Paz et al., 2018). Our new geochemical analyses and correlations suggest that a consolidate and mature volcanic arc developed toward the Oligocene, characterized by calc-alkaline lavas with higher slab contributions and a marked arc signature. This Oligocene magmatic arc developed in the Main Cordillera including the El Maitén Belt volcanism (Las Bayas Section, 33 Ma; Figs. 5, 6 and 7) and the Auca Pan Formation (~39°S, 28 Ma; Iannelli et al., 2017; Rapela et al., 1988), and in the present forearc zone, the initial stages of the Coastal Magmatic belt (~42° S, ~39-37 Ma; Henríquez Ascencio, 2016; López-Escobar & Vergara, 1997; Muñoz et al., 2000; Figures 7 and 8a,c).

Traditional plate reconstructions have proposed an oblique subduction of the Farallon plate beneath the South American margin during the middle Eocene to late Oligocene period (47–28 Ma; Somoza & Ghidella, 2005). However, new plate reconstructions show a higher complexity with two stages; first, low convergence rates and low obliquity (37–33 Ma), followed by a second stage with increasing convergence rates and high obliquity (32–28 Ma) (Matthews et al., 2016; Figure 8b). In this context, we found that the geochemical signature of arc-related volcanism of the El Maitén Belt evolves in accordance with these changes: During the first stage, the subduction at low convergence rates may have conditioned the initial development and limited extent of the tholeiitic arc magmatism, while the development of a more mature arc activity coincides with higher convergence rates at oblique angles by 32 Ma (Figure 8c; Matthews et al., 2016).

6.2.2 Late Oligocene-early Miocene: widespread extension and magmatism (Ventana-Ñireco section)

During late Oligocene-early Miocene times, magmatic activity of variable signature developed all along the Andean margin in direct association with extensional fore-, intra-, and retro-arc basins: Abanico basin (33–36°S; Charrier et al., 1996, 2002; Kay et al., 2005), Cura Mallin basin (36–39°S; Jordan et al., 2001; Radic, 2010), Ñirihuau basin (41–43°S; Bechis et al., 2014; Cazau et al., 2005), and Traiguén basin (45–46°S; Encinas et al., 2016; Hervé et al., 1995). Volcanic activity in the Main Patagonian Cordillera comprises the ~23 to 19 Ma El Maitén Belt (Ventana-Ñireco section), which develops as the initial infill of the Ñirihuau basin, meanwhile Pacific and Atlantic-derived transgressions coexisted with volcanic activity (Bechis et al., 2014; Cazau et al., 2005). Contrarily to the older arc-related volcanic rocks of the Las Bayas section, the lower Miocene tholeiitic basalts from the Ventana-Ñireco section show an E-MORB-like signature with limited slab contributions. These rocks constitute a backarc volcanism with a limited arc signal or a remnant arc signature, which decreases toward the younger pulses of the sequence (Figure 7). Moreover, this sequence is intruded by a probably slightly younger alkaline sills with an OIB signature, originated from a different magma source.

In a regional context, coeval magmatic units located in the present-day forearc zone comprise the subduction-related tholeiitic pillow basalts of the Traiguén Formation (26–23 Ma;

Encinas et al., 2016; Hervé et al., 1995; Silva, 2003) and the mainly andesitic to dacitic volcanism of the Coastal Magmatic Belt (~29–18 Ma; Henríquez Ascencio, 2016; López-Escobar & Vergara, 1997; Muñoz et al., 2000). These arc-related volcanic units are located in a western position regarding the late Eocene-early Oligocene arc locus, and show higher slab contributions (e.g., higher Ba/Ta, La/Ta and Th/Yb ratios; Figure 7) than the outcrops of the El Maitén Belt located toward the east (~23–19 Ma; Ventana-Ñireco section and equivalents). Th_N versus Nb_N diagram highlights these geochemical differences: while these volcanic units located on the forearc zone plot in the volcanic arc field, Miocene samples from the El Maitén Belt show a shift toward backarc fields. These data suggest that arc volcanism migrated westward to the present-day Pacific coastal zone during lower Miocene times (Encinas et al., 2016; Muñoz et al., 2000). Both the Traiguén Formation and the Coastal Magmatic Belt include not only subduction-related volcanic products, but also rocks with OIB affinity (Muñoz et al. 2000; Silva, 2003), which highlight the geochemical variability of magmatism during this stage.

Several authors interpreted a rollback scenario of the Nazca plate in order to explain the retraction of the volcanic front toward the trench, the variability in the signature of the magmas and the development of intra, fore-, and retro-arc basins (Encinas et al., 2016; de Ignacio et al., 2001; Muñoz et al., 2000). Recently, the subduction model proposed by Fennell et al. (2018; based on Quinteros & Sobolev, 2013), supports an accelerated slab rollback for a large portion of the late Oligocene-early Miocene Andean margin (27–46° S) after the subduction of the Aluk-Farallon ocean ridge. In this model, the interaction between the subducted slab and the mantle transition zone at ~410 km increased the slab-pull forces, which triggered an accelerated retreat of the trench hinge away from the upper plate and a steepening of the slab, promoting the onset of an extensional regime at around 24 Ma. However, it is worth noting that this differs from recent plate reconstructions that show higher convergence rates from 32 Ma, which suggests that slab-pull forces could have incremented earlier, producing accelerated roll back before the breakup of Farallon pate (Lonsdale, 2005; Matthews et al., 2016). These models invoke the trenchward migration of the volcanic front that resulted in the development of the Coastal Magmatic Belt and Traiguén Formation arc volcanism, while the widespread extensional regime would have triggered decompression melting in the retroarc zone forming part of the younger sequences of the El Maitén Belt (Ventana-Ñireco section; Figure 8d).

In the foreland region, coeval Somuncura mafic plateau (~29–16 Ma) is characterized by a distinctive intraplate signature (e.g., low Ba/Ta, La/Ta, Th_N and high Ta/Yb and Ta_N; Figure 7), although with relatively higher Ba, Sr and Th than expected for a within plate setting (Kay et al., 2007). It should be noted that Somuncura lava flows share the same geochemical OIB signature of the basaltic sill that intrudes the upper member of Ventana-Ñireco section (~23–19 Ma; Figure 7). This coincidence raises the question of why OIB intrusions took place in the Main Patagonian Cordillera at approximately 20–13 Ma and why Somuncura magmas recorded the presence of subducted components ~800 km east of the trench between ~27–25 Ma (Kay et al., 2007).

An intriguing feature of North Patagonian evolution is the variable geochemical compositions of the widespread magmatic products, which include rocks with variable slab contributions and alkaline rocks with OIB affinity. Though most of the models agree with the slab rollback model, the variable magmatic response has been associated with different processes: Muñoz et al. (2000) explain the signature of the Coastal Magmatic Belt (39-37?, 29–18 Ma), located in the present forearc zone, with the development of a slab window after the subduction of

the Aluk-Farallon mid-ocean ridge. However, as seen in the previous section, after ridge subduction magmatic arc activity resumes and consolidates forming part of the late Eocene-early Oligocene El Maitén Belt volcanic front (e.g., Las Bayas section) without influence of the Paleocene-middle Eocene slab window (Fernández Paz et al., 2018; Iannelli et al., 2017). Other models focused mainly on Somuncura mafic volcanism (~29–16 Ma) in the foreland, e.g. the model of de Ignacio et al. (2001), suggested that the sudden change in the angle of convergence during the breakup of the Farallon plate induced a favorable slab topography to asthenospheric upwellings. Kay et al. (2007), on the other hand, attribute this volcanism to a plume-like mantle upwelling that assimilated subducted components from a disrupted subducted slab. The presence of a plume-like upwelling is certainly difficult to explain as there is no pattern in space and time that can relate this magmatism to a known hotspot (Kay et al., 2007). In this sense, recent works explain atypical plume-like structures and focused upwellings by means of models that associate decompression melting with slab-induced mantle circulation (Faccena et al., 2010 and references therein). This supports de Ignacio et al. (2001) motion that suggests that the slab rollback phenomena and a curved topography in the subducting plate, associated to the change from oblique to orthogonal plate convergence in the late Oligocene, would have resulted in a hot asthenospheric mantle intake, decompression melting and the extrusion of the Somuncura mafic plateau. Furthermore, the numerical model of Fennell et al. (2018) for the Andean margin shows that the invigorated mantle convection promoted by slab rollback could allow the transport of fluids/materials up to ~800 km from the trench, supporting the presence of subducted components in Somuncura magma source. Despite this, this model does not certainly explain the presence of rocks with OIB affinity in association with the arc and backarc volcanic rocks of the Traiguén Formation, Coastal Magmatic Belt and El Maitén Belt located in the forearc and retroarc zones.

As seen in multiple subduction zones around the world, the occurrence of OIB magmatism is not an uncommon process during the development of backarc basins, where arc-related basalts, OIB and MORB-like basalts frequently coexist, being though most typical of island arcs or thinned continental crust (Gao et al., 2018; Pearce & Stern, 2006; Rossel et al. 2013; Smith, 1992; among others). The coexistence of different mantle sources is often associated with decompression melting of undepleted domains present in heterogeneous mantle wedges; such as prevalent, OIB-type or metasomatized subcontinental lithospheric mantle within the mantle wedge (Rossel et al. 2013; Turner et al. 2017; and references therein).The coexistence of different mantle sources is often associated with decompression melting of undepleted domains present in heterogeneous mantle wedges; such as prevalent, OIB-type or subcontinental lithospheric mantle within the mantle wedge (Rossel et al. 2013; Turner et al. 2017; and references therein).In this regard, it is proposed that during periods of slab rollback and ultrafast subduction (>12 cm/y), downward circulation of mantle materials from the overlying mantle wedge is enhanced and requires a return flow in the mantle behind the arc. Under such conditions, induced flow in the mantle wedge may control the progressive replenishment of the mantle wedge, while the increased temperatures as a consequence of higher velocities of the mantle flow could also promote upward flux of material from significant depths (Brandl et al., 2017; Faccena et al., 2010; Gao et al. 2018, Kincaid and Griffiths, 2003, 2004; Staudigel & King, 1992). The occurrence of replenishment of the mantle wedge and the possibility of an upward flux of material from significant depths certainly explains the occurrence of arc related volcanism coexisting with rocks with OIB signature, observed in the intraarc Coastal Magmatic Belt and Traiguén Formation and retroarc magmatism of the lower Miocene El Maitén Belt (Figure 8d). Besides, the model of slab rollback and ultrafast subduction supports also the transport of fluids/materials far from

the trench together with upwellings of hot asthenospheric mantle in the foreland zone required for the development of Somuncura mafic volcanism.

7 Conclusions

The long-standing magmatic activity of the El Maitén Belt records different geochemical trends from late Eocene to early Miocene times, in association with different tectonic stages in the evolution of Andean arc magmatism.

Lower Oligocene volcanic sequences in the Las Bayas range comprise mainly porphyritic basaltic andesites and autobreccias, with interbedded tuffs, dated at 33 Ma (zircon U-Pb age). Geochemical analyses characterize them as andesites and dacites of the calc-alkaline series. Trace elements patterns and ratios, together with isotopic results and AFC models, suggest magmas evolved by assimilation-fractional crystallization with slab (fluid and sediments) and about 30% of crustal contributions (Paleozoic basement).

Early Miocene sequences in the Ventana and Ñireco hills comprise andesitic and dacitic lava flows in the lower section that turns mostly into pyroclastic rocks, volcanic breccias and conglomerates in the middle section. Toward the upper section, mafic lavas intercalate with marine deposits and sill intrusions. Geochemically, mafic lavas can be described as E-MORB-like tholeiites, with minor arc signature and trace elements composition that resemble a backarc setting. Trace element and isotopic compositions suggest that they were generated by low degree of melting (~5%) of a spinel-lherzolite source at low depths within a thin crust. On the other hand, OIB intrusions are alkaline tephrite-basanites with a garnet-bearing magmatic source.

In the regional context, the evolution of the El Maitén Belt from the late Eocene tholeiitic magmatism to the Oligocene mature arc front with higher slab contributions was driven by the oblique subduction at higher convergence rates of the Farallon plate, prior to the breakup of the plate into Nazca and Cocos plates. Then, the early Miocene sequences of El Maitén Belt comprise a retroarc volcanism, associated with marine transgressions, which developed during a stage of widespread extensional conditions. This stage coincides with the breakup of the Farallon plate and the change in the subduction zone configuration into a normal convergence at high rates. Our studies support the model of accelerated Nazca plate rollback in which slab retreat would have promoted a vigorous mantle convection. As a consequence, the volcanic front migrated towards the trench (Coastal Magmatic Belt and Traiguén Formation) and decompression melting in the retroarc zone led to the development of the youngest volcanism of the El Maitén Belt, in accordance with widespread extensional conditions and marine transgressions. Besides, this subduction-induced mantle flow would have allowed the transport of fluids/materials far from the trench together with upwellings of hot asthenospheric mantle in the foreland zone (Somuncura mafic plateau). Likewise, an induced return flow may have favored the income of deep sourced magmas into the mantle wedge, explaining the coexistence of subduction-related volcanism with rocks of OIB affinity both in the arc and the retroarc zone.

Acknowledgements

Raw data and complementary files are in the supporting information and in Mendeley Data repository (http://dx.doi.org/10.17632/pvwnmrvkg8.1). This work was financially supported by CONICET (grant 11220150100426CO), University of Buenos Aires (grant UBACYT 20020150100166BA), ANPCyT PICT-2012-1490, PICT-2014-2240, PICT-2017-3259, and

Fondecyt1151146. The authors acknowledge Juan Otamendi, Eugenio Aragón and Victor Ramos for fruitful discussion. We also thank Lucas Fennell and Sofía Iannelli for discussions and comments on the manuscript, and Sebastián Oriolo for his contributions to this study in relation to the basement composition. This is the contribution number XXX of the Instituto de Estudios Andinos Don Pablo Groeber.

References

Aitcheson, S.J., Harmon, R.S., Moorbath, S., Schneider, A., Soler, P., Soria-Escalante, E., Steele, G., Swainbank, I., Wörner, G. (1995). Pb isotopes define basement domains in the Altiplano, central Andes. Geology 23, 555–558.

Aragón, E., Pinotti, L., D'eramo, F., Castro, A., Rabbia, O., Coniglio, J., … Aguilera, Y. E. (2013). The Farallon-Aluk ridge collision with South America: Implications for the geochemical changes of slab window magmas from fore- to back-arc. Geoscience Frontiers, 4(4), 377–388. https://doi.org/10.1016/j.gsf.2012.12.004

Aragón, E., Castro, A., Díaz-Alvarado, J., & Liu, D.-Y. (2011a). The North Patagonian batholith at Paso Puyehue (Argentina-Chile). SHRIMP ages and compositional features. Journal of South American Earth Sciences, 32(4), 547–554. https://doi.org/10.1016/j.jsames.2011.02.005

Aragón, E., D'Eramo, F., Castro, A., Pinotti, L., Brunelli, D., Rabbia, O., … Ribot, A. (2011b). Tectono-magmatic response to major convergence changes in the North Patagonian suprasubduction system; the Paleogene subduction-transcurrent plate margin transition. Tectonophysics, 509(3–4), 218–237. https://doi.org/10.1016/j.tecto.2011.06.012

Ardolino, A. & Franchi, M. (1993). El vulcanismo Cenozoico de la Meseta Somún Curá, Río Negro y Chubut. XII Congreso Geológico Argentino Actas 4, 225–235.

Asiain, L., Gargiulo, M. F., Reitinger, J., & Ntaflos, T. (2017). Petrografía y geoquímica de lavas básicas del sector noroeste de la meseta de Somuncurá , provincia de Río Negro. Revista de La Asociación Geológica Argentina, 74(4), 570–582.

Baker, M. B., & Stolper, E. M. (1994). Determining the composition of high-pressure mantle melts using diamond aggregates. Geochimica et Cosmochimica Acta, 58(13), 2811-2827.

Bechis, F., Encinas, A., Concheyro, A., Litvak, V. D., Aguirre-Urreta, B., & Ramos, V. A. (2014). New age constraints for the Cenozoic marine transgressions of northwestern Patagonia, Argentina (41°-43°S): Paleogeographic and tectonic implications. Journal of South American Earth Sciences, 52, 72–93. https://doi.org/10.1016/j.jsames.2014.02.003

Bechis, F., Encinas, A., Valencia, V.A., Ramos, V.A. (2015). Analyzing the transition from extension to contraction at the North Patagonian Andes. XIV Congreso Geológico Chileno, La Serena, Chile, Extended Abstracts: 737-739.

Benedini, L., Geraldes, M., Gregori, D. A., Strazzere, L., Marcos, P., & Barros, M. (2017). Nueva edad U-Pb Eocena tardía para la Formación Ventana, Andes Nordpatagónicos,

Provincia de Río Negro. In XX Congreso Geológico Argentino (Vol. Simposio 9, pp. 7–11). San Miguel de Tucumán.

Bilmes, A., Elia, L. D., Franzese, J. R., Veiga, G. D., Hernández, M., D'Elia, L., … Hernández, M. (2013). Miocene block uplift and basin formation in the Patagonian foreland: The Gastre Basin, Argentina. Tectonophysics, 601(August), 98–111. https://doi.org/10.1016/j.tecto.2013.05.001

Bouhier, V. E., Franchini, M. B., Caffe, P. J., Maydagán, L., Rapela, C. W., & Paolini, M. (2017). Petrogenesis of volcanic rocks that host the world-class Ag–Pb Navidad District, North Patagonian Massif: Comparison with the Jurassic Chon Aike Volcanic Province of Patagonia, Argentina. Journal of Volcanology and Geothermal Research, 338, 101–120. https://doi.org/10.1016/j.jvolgeores.2017.03.016

Brown, G. C., Thorpe, R. S., & Webb, P. C. (1984). The geochemical characteristics of granitoids in contrasting arcs and comments on magma sources. Journal of the Geological Society, 141(3), 413–426. https://doi.org/10.1144/gsjgs.141.3.0413

Cande, S. C., & Leslie, R. B. (1986). Late Cenozoic Tectonics of the Southern Chile Trench. Geophysical Research, 91(B1), 471–496.

Castro, A., Moreno-Ventas, I., Fernández, C., Vujovich, G., Gallastegui, G., Heredia, N., … Liu, D. Y. (2011). Petrology and SHRIMP U-Pb zircon geochronology of Cordilleran granitoids of the Bariloche area, Argentina. Journal of South American Earth Sciences, 32(4), 508–530. https://doi.org/10.1016/j.jsames.2011.03.011

Cazau, L., Cortiñas, J., Reinante, S., Asensio, M., Bechis, F., & Apreda, D. (2005). Cuenca De Ñirihuau. In VI Congreso de Exploración y Desarrollo de Hidrocarburos (p. 24). Mar del Plata.

Cazau, L., Mancini, S., Cangini, J., Spalletti, L. A., & Chebli, G. (1989). Cuenca de Ñirihuau. In Cuencas sedimentarias argentinas (Vol. 6). JOUR, Instituto Superior de Correlación Geológica, Universidad Nacional de Tucumán San Miguel de Tucumán.

Cembrano, J., & Lara, L. (2009). The link between volcanism and tectonics in the southern volcanic zone of the Chilean Andes: A review. Tectonophysics, 471(1–2), 96–113. https://doi.org/10.1016/j.tecto.2009.02.038

Chang, Z., Vervoort, J. D., McClelland, W. C., & Knaack, C. (2006). U-Pb dating of zircon by LA-ICP-MS. Geochemistry, Geophysics, Geosystems, 7(5), 1–14. https://doi.org/10.1029/2005GC001100

Chapman, J. B., Ducea, M. N., Kapp, P., Gehrels, G. E., & DeCelles, P. G. (2017). Spatial and temporal radiogenic isotopic trends of magmatism in Cordilleran orogens. Gondwana Research, 48, 189–204. https://doi.org/10.1016/j.gr.2017.04.019

Chapman, J. B., Ducea, M. N., DeCelles, P. G., & Profeta, L. (2015). Tracking changes in crustal thickness during orogenic evolution with Sr/Y: An example from the North American Cordillera. Geology, 43(10), 919–922. https://doi.org/10.1130/G36996.1

Charrier, R., Wyss, A. R., Flynn, J. J., Swisher, C. C., Norell, M. A., Zapatta, F., … Novacek, M. J. (1996). New evidence for late mesozoic-early Cenozoic evolution of the Chilean Andes

in the upper Tinguiririca valley (35 °S), central Chile. Journal of South American Earth Sciences, 9(5–6), 393–422. https://doi.org/10.1016/S0895-9811(96)00035-1

Charrier, R., Baeza, O., Elgueta, S., Flynn, J. J., Gans, P., Kay, S. M., … Zurita, E. (2002). Evidence for Cenozoic extensional basin development and tectonic inversion south of the flat-slab segment, southern Central Andes, Chile (33??-36??S.L.). Journal of South American Earth Sciences, 15(1), 117–139. https://doi.org/10.1016/S0895-9811(02)00009-3

Chiaradia, M. (2015). Crustal thickness control on Sr/Y signatures of recent arc magmas: an Earth scale perspective. Scientific Reports, 5, 8115. https://doi.org/10.1038/srep08115

Coira, B., Franchi, M. & Nullo, F. E. (1985). Vulcanismo terciario al oeste de Somuncurá y su relación con el arco magmático de la Cordillera Nordpatagónica, Argentina. IV Congreso Geológico Chileno Actas 4, 68–88.

Corbella, H. (1982a). Complejo volcánico alcalino Sierra de Telsen, Patagonia extraandina, Argentina. V Congreso Latinoamericano de Geología Actas 2, 225–238.

Corbella, H. (1982b). Quimismo del complejo volcánico alcalino Sierra Negra de Telsen, Patagonia extrandina norte, Argentina. 1 Elementos mayores. Asociación Argentina de Mineralogía, Petrología y Sedimentología Revista 13, 29–38.

Creaser, R. A., Gru, H., Carlson, J., & Crawford, B. (2004). Macrocrystal phlogopite Rb – Sr dates for the Ekati property kimberlites , Slave Province , Canada : evidence for multiple intrusive episodes in the Paleocene and Eocene, 76, 399–414. https://doi.org/10.1016/j.lithos.2004.03.039

Cross, T. A., & Pilger, R. H. (1982). Controls of subduction geometry location of magmatic arcs and tectonics of arc and back-arc regions. Geological Society of America Bulletin, 93(6), 545–562. https://doi.org/10.1130/0016-7606(1982)93<545:COSGLO>2.0.CO;2

Dalla Salda, L., Cingolani, C. A., & Varela, R. (1991). El basamento pre-andino igneo metamorfico de San Martin de los Andes, Neuquén. Asociación Geológica Argentina, 44(3–4), 223–234.

Dalla Salla, L., Leguizawjn, M., Mazzoni, M., Rapela, C., & Spalletti, L. (1981). Características del vulcanismo paleógeno en la cordillera Nordpatagónica entre las latitudes 39° 30’ y 41° 20’ S. In VIII Congreso Geológico Argentino (pp. 629–657). San Luis.

Davidson, J., Turner, S., Handley, H., Macpherson, C., & Dosseto, A. (2007). Amphibole “sponge” in arc crust? Geology, 35(9), 787–790. https://doi.org/10.1130/G23637A.1

Davidson, J., Turner, S., & Plank, T. (2013). Dy/Dy*: Variations arising from mantle sources and petrogenetic processes. Journal of Petrology, 54(3), 525–537. https://doi.org/10.1093/petrology/egs076

DeCelles, P. G., Ducea, M. N., Kapp, P., & Zandt, G. (2009). Cyclicity in Cordilleran orogenic systems. Nature Geoscience, 2(4), 251–257. https://doi.org/10.1038/ngeo469

Deniel, C., & Pin, C. (2001). Single-stage method for the simultaneous isolation of lead and strontium from silicate samples for isotopic measurements. Analytica Chimica Acta, 426(1), 95–103. https://doi.org/10.1016/S0003-2670(00)01185-5

DePaolo, D.J. (1981). Trace element and isotopic effects of combined wallrock assimilation and fractional crystallization. Earth and Planetary Science Letters, 53, 189-202.

Dickinson, W. R., & Gehrels, G. E. (2003). U-Pb ages of detrital zircons from Permian and Jurassic eolian sandstones of the Colorado Plateau, USA: Paleogeographic implications. Sedimentary Geology, 163(1–2), 29–66. https://doi.org/10.1016/S0037-0738(03)00158-1

Ducea, M. N., Saleeby, J. B., & Bergantz, G. (2015). The Architecture, Chemistry, and Evolution of Continental Magmatic Arcs. Annual Review of Earth and Planetary Sciences, 43(1), 299–333. https://doi.org/10.1146/annurev-earth-060614-105049

Duhart, P., McDonough, M., Muñoz, J., Martin, M., & Villeneuve, M. (2001). El Complejo Metamórfico Bahía Mansa en la cordillera de la Costa del centro-sur de Chile (39°30'-42°00'S): geocronología K-Ar, 40Ar/39Ar y U-Pb e implicancias en la evolución del margen sur-occidental de Gondwana. Revista Geológica de Chile, 28, 179–208.

Echaurren, A., Oliveros, V., Folguera, A., Ibarra, F., Creixell, C., & Lucassen, F. (2017). Early Andean tectonomagmatic stages in north Patagonia: insights from field and geochemical data. Journal of the Geological Society, 174(3), 405–421. https://doi.org/10.1144/jgs2016-087

Echaurren, A., Folguera, A., Gianni, G., Orts, D. L., Tassara, A., Encinas, A., … Valencia, V. A. (2016). Tectonic evolution of the North Patagonian Andes (41°–44° S) through recognition of syntectonic strata. Tectonophysics, 677, 99–114. https://doi.org/10.1016/j.tecto.2016.04.009

Elgueta, S., & Mpodozis, C. (2012). Evolución tectono-sedimentaria de la cuenca del río Cruces (Valdivia) durante el Neógeno. 13th Congreso Geológico Chileno, 649–651.

Ellam, R. M. (1992). Lithospheric thickness as a control on basalt geochemistry. Geology, 20(2), 153–156. https://doi.org/10.1130/0091-7613(1992)020<0153:LTAACO>2.3.CO;2

Encinas, A., Folguera, A. A., Oliveros, V. V., De Girolamo Del Mauro, L., Tapia, F., Riffo, R., … Álvarez, O. (2016). Late Oligocene-early Miocene submarine volcanism and deep-marine sedimentation in an extensional basin of southern Chile: Implications for the tectonic development of the North Patagonian Andes. Bulletin of the Geological Society of America, 128(5–6), 807–823. https://doi.org/10.1130/B31303.1

Encinas, A., Pérez, F., Nielsen, S. N., Finger, K. L., Valencia, V., & Duhart, P. (2014). Geochronologic and paleontologic evidence for a pacific-atlantic connection during the late oligocene-early miocene in the Patagonian Andes (43-44oS). Journal of South American Earth Sciences, 55, 1–18. https://doi.org/10.1016/j.jsames.2014.06.008

Encinas, A., Finger, K. L., Buatois, L. A., & Peterson, D. E. (2012). Major forearc subsidence and deep-marine Miocene sedimentation in the present Coastal Cordillera and Longitudinal

Depression of south-central Chile (38°30'S-41°45'S). Bulletin of the Geological Society of America, 124(7–8), 1262–1277. https://doi.org/10.1130/B30567.1

Faccenna, C., Becker, T. W., Lallemand, S., Lagabrielle, Y., Funiciello, F., & Piromallo, C. (2010). Subduction-triggered magmatic pulses: A new class of plumes?. Earth and Planetary Science Letters, 299(1-2), 54-68.

Fennell, L. M., Quinteros, J., Iannelli, S. B., Litvak, V. D., & Folguera, A. (2018). The role of the slab pull force in the late Oligocene to early Miocene extension in the Southern Central Andes (27°-46°S): Insights from numerical modeling. Journal of South American Earth Sciences, (2017). https://doi.org/10.1016/j.jsames.2017.12.012

Fernández Paz, L., Litvak, V. D., Echaurren, A., Iannelli, S. B., Encinas, A., Folguera, A., & Valencia, V. (2018). Late Eocene volcanism in North Patagonia (42˚30'-43˚S): Arc resumption after a stage of within-plate magmatism. Journal of Geodynamics, 113, 13–31. https://doi.org/10.1016/j.jog.2017.11.005

Folguera, A., & Ramos, V. A. (2011). Repeated eastward shifts of arc magmatism in the Southern Andes: A revision to the long-term pattern of Andean uplift and magmatism. Journal of South American Earth Sciences, 32(4), 531–546. https://doi.org/10.1016/j.jsames.2011.04.003

Francis, P.W., Sparks, R.S.J., Hawkesworth, C.J., Thorpe, R.S., Pyle, D.M., Tait, S.R., Montovani, M.S., McDermott, F. (1989). Petrology and geochemistry of volcanic rocks of the Cerro Galan caldera, northwest Argentina. Geological Magazine 126, 515–547.

Gao, Z., Zhang, H. F., Yang, H., Pan, F. Bin, Luo, B. J., Guo, L., … Wu, J. (2018). Back-arc basin development: Constraints on geochronology and geochemistry of arc-like and OIB-like basalts in the Central Qilian block (Northwest China). Lithos, 310–311, 255–268. https://doi.org/10.1016/j.lithos.2018.04.002

Giacosa, R. E., & Heredia, N. C. (2004). Structure of the North Patagonian thick-skinned fold-and-thrust belt, southern central Andes, Argentina (41??-42??S). Journal of South American Earth Sciences, 18(1), 61–72. https://doi.org/10.1016/j.jsames.2004.08.006

Giacosa, R. E., Afonso, J. C., Nemesio Heredia, C., & Paredes, J. (2005). Tertiary tectonics of the sub-Andean region of the North Patagonian Andes, southern central Andes of Argentina (41-42°30′S). Journal of South American Earth Sciences, 20(3), 157–170. https://doi.org/10.1016/j.jsames.2005.05.013

González, P. (1994). Mapa Geológico de la Provincia de Río Negro. República Argentina. Escala 1:750.000. Secr. Minería, Dir. Nac. del Serv. Geológico.

González Bonorino, F., & González Bonorino, G. (1978). Geología de la región de San Carlos de Bariloche. Revista de La Asociación Geológica Argentina, 33(3), 175–210.

González Díaz, E. F. (1979). La edad de la Formación Ventana, en el área al norte y al este del lago Nahuel Huapi. Revista de La Asociación Geológica Argentina, 34(2), 113–124.

Gorton, M. P., & Schandl, E. V. A. S. (2000). From Continents To Island Arcs : a Geochemical Index of Tectonic Setting for Arc-Related and Within-Plate Felsic To Intermediate Volcanic Rocks, 38, 1065–1073.

Grove, T., Parman, S., Bowring, S., Price, R., & Baker, M. (2002). The role of an H2O-rich fluid component in the generation of primitive basaltic andesites and andesites from the Mt. Shasta region, N California. Contributions to Mineralogy and Petrology, 142(4), 375–396. https://doi.org/10.1007/s004100100299

Haschke, M., Siebel, W., Günther, A., Scheuber, E. (2002). Repeated crustal thickening and recycling during the Andean orogeny in north Chile (21°–26°S). Journal of Geophysical Research – Solid Earth 107. doi:10.1029/2001JB000328

Hawkesworth, C. J., Turner, S. P., McDermott, F., Peate, D. W., & van Calsteren, P. (1997). U-Th Isotopes in Arc Magmas: Implications for Element Transfer from the Subducted Crust. Science, 276(5312), 551–555. https://doi.org/10.1126/science.276.5312.551

Henríquez Ascencio, G. J. (2016). Petrografía, geoquímica y marco geotectónico del Complejo Volcánico Ancud, Provincia de Chiloé, Región de los Lagos, Chile. Universidad de Concepción.

Hervé, F., Pankhurst, R. J., Drake, R., & Beck, M. E. (1995). Pillow metabasalts in a mid-Tertiary extensional basin adjacent to the Liquiñe-Ofqui fault zone: the Isla Magdalena area, Aysén, Chile. Journal of South American Earth Sciences, 8(1), 33–46. https://doi.org/10.1016/0895-9811(94)00039-5

Hervé, F., Calderón, M., Fanning, C. M., Pankhurst, R. J., & Godoy, E. (2013). Provenance variations in the Late Paleozoic accretionary complex of central Chile as indicated by detrital zircons. Gondwana Research, 23(2), 1122–1135.

Hervé, F., Fuentes, F. J., Calderón, M., Fanning, M., Quezada, P., Pankhurst, R., & Rapela, C. (2017). Ultramafic rocks in the North Patagonian Andes: is their emplacement associated with the Neogene tectonics of the Liquiñe–Ofqui Fault Zone? Andean Geology, 44(1), 1. https://doi.org/10.5027/andgeoV44n1-a01

Hickey-Vargas, R., Holbik, S., Tormey, D., Frey, F. A., & Roa, H. M. (2016). Basaltic rocks from the Andean Southern Volcanic Zone: Insights from the comparison of along-strike and small-scale geochemical variations and their sources. Lithos, 258, 115-132.

Holmden, C., Creaser, R. A., & Muehlenbachs, K. (1997). Paleosalinities in ancient brackish water systems determined by 87S r/86Sr ratios in carbonate fossils: A case study from the Western Canada Sedimentary Basin, 61(10), 2105–2118.

Horton, B. K. (2018). Tectonic regimes of the central and southern Andes: Responses to variations in plate coupling during subduction. Tectonics, 37, 402–429. https://doi.org/10.1002/2017TC004624

Huw Davies, J., & Bickle, M. J. (1991). A physical model for the volume and composition of melt produced by hydrous fluxing above subduction zones. Philosophical Transactions: Physical Sciences and Engineering, 335, 355–364.

Iannelli, S. B., Litvak, V. D., Fernández Paz, L., Folguera, A., Ramos, M. E., & Ramos, V. A. (2017). Evolution of Eocene to Oligocene arc-related volcanism in the North Patagonian

Andes (39–41S), prior to the break-up of the Farallon plate. Tectonophysics, 696–697, 70–87. https://doi.org/10.1016/j.tecto.2016.12.024

de Ignacio, C., López, I., Oyarzún, R., & Márquez, A. (2001). The northern Patagonia Somuncura plateau basalts: a product of slab-induced, shallow asthenospheric upwelling? Terra Nova, 13(2), 117–121.

Irvine, T. N., & Baragar, W. R. A. (1971). A Guide to the Chemical Classification of the Common Volcanic Rocks. Canadian Journal of Earth Sciences, 8(5), 523–548. https://doi.org/10.1139/e71-055

Jacques, G., Hoernle, K., Gill, J., Hauff, F., Wehrmann, H., Garbe-Schönberg, D., … Lara, L. E. (2013). Across-arc geochemical variations in the Southern Volcanic Zone, Chile (34.5-38.0oS): Constraints on mantle wedge and slab input compositions. Geochimica et Cosmochimica Acta, 123, 218–243. https://doi.org/10.1016/j.gca.2013.05.016

Jordan, T. E., Burns, W. M., Veiga, R., Pángaro, F., Copeland, P., Kelley, S., & Mpodozis, C. (2001). Extension and basin formation in the southern Andes caused by increased convergence rate: A mid-Cenozoic trigger for the Andes. Tectonics, 20(3), 308–324.

Kay, S. M., & Copeland, P. (2006). Early to middle Miocene backarc magmas of the Neuquén Basin: Geochemical consequences of slab shallowing and the westward drift of South America. Geological Society of America Special Papers, 407(09), 185–213. https://doi.org/10.1130/2006.2407(09)

Kay, S. M., Jones, H. A., & Kay, R. W. (2013). Origin of Tertiary to Recent EM- and subduction-like chemical and isotopic signatures in Auca Mahuida region (37°-38°S) and other Patagonian plateau lavas. Contributions to Mineralogy and Petrology, 166(1), 165–192. https://doi.org/10.1007/s00410-013-0870-9

Kay, S. M., Godoy, E., & Kurtz, A. (2005). Episodic arc migration, crustal thickening, subduction erosion, and magmatism in the south-central Andes. Geological Society of America Bulletin, 117(1–2), 67–88. https://doi.org/10.1130/B25431.1

Kay, S. M., Ardolino, A. A., Gorring, M. L., & Ramos, V. A. (2007). The Somuncura Large Igneous Province in Patagonia : Interaction of a Transient Mantle Thermal Anomaly with a Subducting Slab. Journal of Petrology, 48, 1–35. https://doi.org/10.1093/petrology/egl053

Kincaid, C., & Griffith, R.W. (2003). Laboratory models of the thermal evolution of the mantle during rollback subduction. Nature 425, 58–62

Kincaid, C., & Griffiths, R. W. (2004). Variability in flow and temperatures within mantle subduction zones. Geochemistry, Geophysics, Geosystems, 5(6), 1–20. https://doi.org/10.1029/2003GC000666

Lallemand, S., Heuret, A., Boutelier, D., Cedex, M., & Boutelier, D. (2005). On the relationships between slab dip, back-arc stress, upper plate absolute motion, and crustal

nature in subduction zones. Geochemistry, Geophysics, Geosystems, 6. https://doi.org/10.1029/2005GC000917

Lara, L., Rodríguez, C., Moreno, H., & Pérez de Arce, C. (2001). Geocronología K-Ar y geoquímica del volcanismo plioceno superior-pleistoceno de los Andes del sur (39-42°S). Revista Geológica de Chile. https://doi.org/10.4067/S0716-02082001000100004

Lavenu, A., & Cembrano, J. (1999). Compressional- and transpressional-stress pattern for Pliocene and Quaternary brittle deformation in fore arc and intra-arc zones (Andes of Central and Southern Chile). Journal of Structural Geology, 21(12), 1669–1691. https://doi.org/10.1016/S0191-8141(99)00111-X

Lister, G. S., Forster, M. A., & Rawling, T. J. (2001). Episodicity during orogenesis. Continental Reactivation and Reworking, 184(1), 89–113. https://doi.org/10.1144/GSL.SP.2001.184.01.06

Lindsay, J.M., Schmitt, A.K., Trumbull, R.B., de Silva, S.L., Siebel, W., Emmermann, R. (2001). Magmatic evolution of the La Pacana Caldera system, central Andes, Chile: compositional variation of two cogenetic, large-volume felsic ignimbrites and implications for contrasting eruption mechanisms. Journal of Petrology 42, 459–486.

Lizuain, A., Ragona, D., Folguera, A. (1995). Mapa geológico de la provincia del Chubut, escala 1: 750.000. Secr. Minería Dir. Nac. del Serv. Geol.

Lonsdale, P. (2005). Creation of the Cocos and Nazca plates by fission of the Farallon plate. Tectonophysics, 404(3–4), 237–264. https://doi.org/10.1016/j.tecto.2005.05.011

López-Escobar, L., Parada, M. A., Moreno, H., Frey, F. A., & Hickey-Vargas, R. (1992). A contribution to the petrogenesis of Osorno and Calbuco volcanoes, Southern Andes (41°00'-41°30'8): comparative study. Revista Geológica de Chile, 19(2), 211–226.

López-Escobar, L., Cembrano, J., & Moreno, H. (1995). Geochemistry and tectonics of the Chilean southern Andes basaltic Quaternary volcanism (37-46°S). Revista Geológica de Chile, 22(2), 219–234. https://doi.org/10.5027/andgeoV22n2-a06

López-Escobar, L., Kilian, R., Kempton, P. D., & Tagiri, M. (1993). Petrography and geochemistry of Quaternary rocks from the Southern Volcanic Zone of the Andes between 41°30' and 46°00'S, Chile. Revista Geológica de Chile, 20(1), 33–55. https://doi.org/10.5027/andgeoV20n1-a04

López-Escobar, L., & Vergara, M. (1997). Eocene-Miocene Longitudinal Depression and Quaternary Volcanism In the Southern Andes, Chile (33-42.5oS): a geochemical comparison. Revista Geológica de Chile, 24(2), 227–244.

Lucassen, F., Trumbull, R., Franz, G., & Creixell, C. (2004). Distinguishing crustal recycling and juvenile additions at active continental margins : the Paleozoic to recent compositional evolution of the Chilean Pacific margin (36 – 41 8 S) q. Journal of South American Earth Sciences, 17, 103–119. https://doi.org/10.1016/j.jsames.2004.04.002

Ludwig, K. R. (2003). User's manual for Isoplot 3.00: a geochronological toolkit for Microsoft Excel. BOOK, Kenneth R. Ludwig.

Malumián, N., & Náñez, C. (2011). The Late Cretaceous-Cenozoic transgressions in Patagonia and the Fuegian Andes: Foraminifera, palaeoecology, and palaeogeography. Biological Journal of the Linnean Society, 103(2), 269–288. https://doi.org/10.1111/j.1095-8312.2011.01649.x

Mamani, M., Wörner, G., & Sempere, T. (2010). Geochemical variations in igneous rocks of the Central Andean orocline (13 ° S to 18 ° S): Tracing crustal thickening and magma generation through time and space, (1), 162–182. https://doi.org/10.1130/B26538.1

Mantle, G. W., & Collins, W. J. (2008). Quantifying crustal thickness variations in evolving orogens : Correlation between arc basalt composition and Moho depth, (1), 87–90. https://doi.org/10.1130/G24095A.1

Marshall, L. G., Hoffstetter, R. & Pascual, R. (1983). Geochronology of the continental mammal-bearing Tertiary of South America. Palaeovertebrate, Memoir Extra, pp 93.

Marshall, L. G., Cifelli, R. L., Drake, R. E. & Curtis, G. H. (1986). Vertebrate paleontology, geology, and geochronology of the Tapera de López and Scarritt Pocket, Chubut province, Argentina. Journal of Paleontology 60, 920–951.

Matthews, K. J., Maloney, K. T., Zahirovic, S., Williams, S. E., Seton, M., & Müller, R. D. (2016). Global plate boundary evolution and kinematics since the late Paleozoic. Global and Planetary Change, 146(January 2017), 226–250. https://doi.org/10.1016/j.gloplacha.2016.10.002

Maury, R. C., Defant, M. J., & Joron, J. L. (1992). Metasomatism of the sub-arc mantle inferred from trace elements in Philippine xenoliths. Nature, 360(6405), 661–663. https://doi.org/10.1038/360661a0

McDonough, W. F., & Sun, S. (1995). The composition of the Earth. Chemical Geology, 120(3–4), 223–253. https://doi.org/10.1016/0009-2541(94)00140-4

McKenzie, D., & O'Nions, R. K. (1991). Partial melt distribution from inversion of rare earth element concentrations. Journal of Petrology, 32, 1021–1091. https://doi.org/10.1093/petrology/32.5.1021

Mella, M., Muñoz, J., Vergara, M., Klohn, E., Farmer, L., & Stern, C. R. (2005). Petrogenesis of the Pleistocene Tronador Volcanic Group, Andean Southern Volcanic Zone. Revista Geológica de Chile, 32(1), 1–21. https://doi.org/10.4067/S0716-02082005000100008

Menzies, M. A., Leeman, W. P., & Hawkesworth, C. J. (1983). Isotope geochemistry of Cenozoic volcanic rocks reveals mantle heterogeneity below western USA. Nature, 303(5914), 205–209. https://doi.org/10.1038/303205a0

Míková, J., & Denková, P. (2007). Modified chromatographic separation scheme for Sr and Nd isotope analysis in geological silicate samples. Journal of Geosciences, 52(3–4), 221–226. https://doi.org/10.3190/jgeosci.015

Miyashiro, A. (1974). Volcanic rock series in island arcs and active continental margins. American Journal of Science, 274(4), 321–355. JOUR.

Muñoz, J., Troncoso, R., Duhart, P., Crignola, P., Farmer, L., & Stern, C. R. (2000). The

relation of the mid-Tertiary Coastal Magmatic Belt in south-central Chile to the late Oligocene increase in plate convergence rate. Revista Geológica de Chile, 27(2), 177–203. https://doi.org/10.4067/S0716-02082000000200003

Nakamura, N. (1974). Determination of REE, Ba, Fe, Mg, Na and K in carbonaceous and ordinary chondrites. Geochimica et Cosmochimica Acta, 38(5), 757–775. https://doi.org/10.1016/0016-7037(74)90149-5

Ort, M.H., Coira, B.L., Mazoni, M.M. (1996). Generation of a crust-mantle magma mixture: magma sources and contamination at Cerro Panizoz, central Andes. Contributions to Mineralogy and Petrology 123, 308–322.

Orts, D. L., Folguera, A., Giménez, M., Ruiz, F., Rojas Vera, E. A., Lince Klinger, F., … Lince Klinger, F. (2015). Cenozoic building and deformational processes in the North Patagonian Andes. Journal of Geodynamics, 86, 26–41. https://doi.org/10.1016/j.jog.2015.02.002

Orts, D. L., Folguera, A., Encinas, A., Ramos, M. E., Tobal, J., & Ramos, V. A. (2012). Tectonic development of the North Patagonian Andes and their related Miocene foreland basin (41°30 ′ -43°S). Tectonics, 31, 1–24. https://doi.org/10.1029/2011TC003084

Paces, J. B., & Miller, J. D. (1993). Precise U-Pb ages of Duluth Complex and related mafic intrusions, northeastern Minnesota: Geochronological insights to physical, petrogenetic, paleomagnetic, and tectonomagmatic processes associated with the 1.1 Ga Midcontinent Rift System. Journal of Geophysical Research: Solid Earth, 98(B8), 13997–14013. https://doi.org/10.1029/93JB01159

Pankhurst, R. J., Weaver, S. D. D., Hervé, F., & Larrondo, P. (1999). Mesozoic – Cenozoic Evolution of the North Patagonian Batholith in Aysén , Southern Chile. Journal of the Geological Society, London, 156, 673–694. https://doi.org/10.1144/gsjgs.156.4.0673

Pankhurst, R. J., Rapela, C. W., Fanning, C. M., & Márquez, M. (2006). Gondwanide continental collision and the origin of Patagonia. Earth-Science Reviews, 76(3–4), 235–257. https://doi.org/10.1016/j.earscirev.2006.02.001

Parada, M. A., López-Escobar, L., Oliveros, V., Fuentes, F., Morata, D., Calderón, M., … Moreno, H. (2007). Andean magmatism. In The geology of Chile.

Pearce, J. A. (1983). Role of the sub-continental lithosphere in magma genesis at active continental margins.

Pearce, J. A., & Parkinson, I. J. (1993). Trace element models for mantle melting: application to volcanic arc petrogenesis. Geological Society, London, Special Publications, 76(1), 373–403. https://doi.org/10.1144/GSL.SP.1993.076.01.19

Pearce, J. A., & Stern, R. J. (2006). Origin of Back-Arc Basin Magmas: Trace Element and Isotope Perspectives. Back-Arc Spreading Systems: Geological, Biological, Chemical, and Physical Interactions, 63–86. https://doi.org/10.1029/166GM06

Petford, N., Cheadle, M., & Barreiro, B. (1996). Age and origin of southern patagonian flood basalts, Chile Chico region (46o45'S). In Third ISAG (Vol. 17, pp. 629–632). St Malo (France).

Pin, C., & Zalduegui, J. S. (1997). Sequential separation of light rare-earth elements, thorium and uranium by miniaturized extraction chromatography: application to isotopic analyses of silicate rocks. Analytica Chimica Acta, 339(1–2), 79–89.

Plank, T. (2005). Constraints from Thorium / Lanthanum on Sediment Recycling at Subduction Zones and the Evolution of the Continents, 46(5), 921–944. https://doi.org/10.1093/petrology/egi005

Profeta, L., Ducea, M. N., Chapman, J. B., Paterson, S. R., Gonzales, S. M. H., Kirsch, M., … DeCelles, P. G. (2015). Quantifying crustal thickness over time in magmatic arcs. Scientific Reports, 5(17786). https://doi.org/10.1038/srep17786

Quinteros, J., & Sobolev, S. V. (2013). Why has the Nazca plate slowed since the Neogene? Geology, 41(1), 31–34. https://doi.org/10.1130/G33497.1

Radic, J. P. (2010). Las cuencas cenozoicas y su control en el volcanismo de los Complejos Nevados de Chillán y Copahue-Callaqui (Andes del sur, 36-39??S). Andean Geology, 37(1), 220–246. https://doi.org/10.4067/S0718-71062010000100009

Radic, J. P., Álvarez, P., Rojas, L., Czollak, C., Parada, R., & Ortiz, V. (2009). La cuenca de Valdivia como parte del sistema de antearco de la plataforma continental de Chile central entre los 36° y 40° S. In XII Congreso Geológico Chileno (pp. 22–26). Santiago, Chile.

Ramos, M. E., Tobal, J., Sagripanti, L., Folguera, A., Orts, D., Giménez, M., & Ramos, V. (2015). The North Patagonian orogenic front and related foreland evolution during the Miocene, analyzed from synorogenic sedimentation and U / Pb dating (~42°S). Journal of South American Earth Sciences, 1–19. https://doi.org/10.1016/j.jsames.2015.08.006

Ramos, V. A. (1982). Las ingresiones pacíficas del terciario en el norte de la Patagonia (Argentina). In III Congreso Geológico Chileno (pp. 262–288). Concepción.

Ramos, V. A., Litvak, V. D., Folguera, A., & Spagnuolo, M. (2014). An Andean tectonic cycle: From crustal thickening to extension in a thin crust (34°-37°SL). Geoscience Frontiers, 5(3), 351–367. https://doi.org/10.1016/j.gsf.2013.12.009

Rapela, C. W., Spalletti, L. A., Merodio, J. C., & Aragón, E. (1988). Temporal evolution and spatial variation of early tertiary volcanism in the Patagonian Andes (40°S-42°30'S). Journal of South American Earth Sciences, 1(1), 75–88. https://doi.org/10.1016/0895-9811(88)90017-X

Rapela, C. W., Pankhurst, R. J., Fanning, C. M., & Herve, F. (2005). Pacific subduction coeval with the Karoo mantle plume : the early Jurassic subcordilleran belt of northwestern Patagonia. Geological Society, (June 2007), 217–239. https://doi.org/10.1144/GSL.SP.2005.246.01.07

Rapela, C. W., Spalletti, L. A., & Merodio, J. C. (1983). Evolución magmática y geotectónica de la "Serie Andesítica" andina (Paleoceno-Eoceno) en la cordillera Nordpatagónica. Revista de La Asociación Geológica Argentina, 38(3–4), 469–484.

Rogers, G., Hawkesworth, C.J. (1989). A geochemical traverse across the North Chilean Andes: evidence for crust generation from the mantle wedge. Earth and Planetary Sciences and Letters 91, 271–285.

Rolando, A. P., Hartmann, L. A., Santos, J. O. S., Fernandez, R. R., Etcheverry, R. O., Schalamuk, I. A., & McNaughton, N. J. (2002). SHRIMP zircon U-Pb evidence for extended Mesozoic magmatism in the Patagonian Batholith and assimilation of Archean crustal components. Journal of South American Earth Sciences, 15(2), 267–283. https://doi.org/10.1016/S0895-9811(02)00015-9

Rossel, P., Oliveros, V., Ducea, M. N., Charrier, R., Scaillet, S., Retamal, L., & Figueroa, O. (2013). The Early Andean subduction system as an analog to island arcs: Evidence from across-arc geochemical variations in northern Chile. Lithos, 179, 211-230.

le Roux, J. P. (2012). A review of Tertiary climate changes in southern South America and the Antarctic Peninsula. Part 1: Oceanic conditions. Sedimentary Geology, 247–248, 1–20. https://doi.org/10.1016/j.sedgeo.2011.12.014

Rudnick, R. L., & Fountain, D. M. (1995). Nature and composition of the continental crust: A lower-crustal perspective. Reviews of Geophysics, 33(3), 267–309. https://doi.org/Doi 10.1029/95rg01302

Saccani, E. (2015). A new method of discriminating different types of post-Archean ophiolitic basalts and their tectonic significance using Th-Nb and Ce-Dy-Yb systematics. Geoscience Frontiers, 6(4), 481–501. https://doi.org/10.1016/j.gsf.2014.03.006

Schellart, W. P. (2008). Subduction zone trench migration: Slab driven or overriding-plate-driven? Physics of the Earth and Planetary Interiors, 170(1–2), 73–88. https://doi.org/10.1016/j.pepi.2008.07.040

Schmidberger, S. S., Simonetti, A., Heaman, L. M., Creaser, R. A., & Whiteford, S. (2007). Lu–Hf , in-situ Sr and Pb isotope and trace element systematics for mantle eclogites from the Diavik diamond mine : Evidence for Paleoproterozoic subduction beneath the Slave craton , Canada, 254, 55–68. https://doi.org/10.1016/j.epsl.2006.11.020

Sernageomin. (2003). Mapa Geológico de Chile: versión digital. Publicación Geológica Digital 4, pp. 25

Shinjo, R., Chung, S.-L., Kato, Y., & Kimura, M. (1999). Geochemical and Sr-Nd isotopic characteristics of volcanic rocks from the Okinawa Trough and Ryukyu Arc: Implications for the evolution of a young, intracontinental back arc basin. Journal of Geophysical Research: Solid Earth, 104(B5), 10591–10608. https://doi.org/10.1029/1999JB900040

Shaw, D.M. (1970). Trace element fractionation during anatexis. Geochimica et Cosmochimica Acta 34, 237-243.

Silva, C. (2003). Ambiente geotectónico de erupción y metamorfismo de metabasaltos almohadillados de los Andes Norpatagónicos (42°- 46° S), Chile. Universidad de Chile.

Smith A.D., 1992. Back-arc convection model for Columbia River Basalt Genesis. Tectonophysics, 207: 269-285.

Somoza, R., & Ghidella, M. E. (2005). Convergencia en el margen occidental de América del sur durante el Cenozoico: Subducción de las placas de Nazca, Farallon y Aluk. Revista de La Asociación Geológica Argentina, 60(4), 797–809. https://doi.org/10.3989/scimar.2002.66n4433

Somoza, R., & Ghidella, M. E. (2012). Late Cretaceous to recent plate motions in western South America revisited. Earth and Planetary Science Letters, 331–332, 152–163. https://doi.org/10.1016/j.epsl.2012.03.003

D'Souza, R. J., Canil, D., & Creaser, R. A. (2016). Assimilation , differentiation , and thickening during formation of arc crust in space and time : The Jurassic Bonanza arc , Vancouver Island , Canada, (3), 543–557. https://doi.org/10.1130/B31289.1

Spalletti, L. A. (1983). Paleogeografía de la Formación Ñirihuau y sus equivalentes en la región occidental de Neuquén, Río Negro y Chubut. Revista de La Asociación Geológica Argentina, 38(3–4), 454–468.

Staudigel, H., & King, S. D. (1992). Ultrafast subduction: the key to slab recycling efficiency and mantle differentiation? Earth and Planetary Science Letters, 109(3–4), 517–530. https://doi.org/10.1016/0012-821X(92)90111-8

Stern, C. R. (2004). Active Andean volcanism: its geologic and tectonic setting. Revista Geológica de Chile, 31(2), 163–206.

Sun, S., & McDonough, W. F. (1989). Chemical and isotopic systematics of oceanic basalts: implications for mantle composition and processes. Geological Society, London, Special Publications, 42(1), 313–345. https://doi.org/10.1144/GSL.SP.1989.042.01.19

Sun, W., Liu, L., Hu, Y., Ding, W., & Liu, J. (2018). Post-ridge-subduction acceleration of the Indian plate induced by slab rollback, 3, 1–7. https://doi.org/10.1016/j.sesci.2017.12.003

Tanaka, T., Togashi, S., Kamioka, H., Amakawa, H., Kagami, H., Hamamoto, T., … Dragusanu, C. (2000). JNdi-1: A neodymium isotopic reference in consistency with LaJolla neodymium. Chemical Geology, 168(3–4), 279–281. https://doi.org/10.1016/S0009-2541(00)00198-4

Tatsumi, Y., & Eggins, S. (1995). Subduction zone magmatism (Vol. 1). Wiley.

Thomson, S. N., & Hervé, F. (2002). New time constraints for the age of metamorphism at the ancestral Pacific Gondwana margin of southern Chile (42-52°S). Revista Geológica de Chile, 29, 255–271.

Tobal, J. E., Vera, E. R., Folguera, A., & Ramos, V. A. (2012). Deformación andina en el cordón del Hielo Azul al oeste de El Bolsón. Implicancias en la evolución tectónica de la Cordillera Norpatagónica en Río Negro, Argentina. Andean Geology, 39(3), 442–463. https://doi.org/10.5027/andgeoV39n3-a05

Turner, S. J., & Langmuir, C. H. (2015). What processes control the chemical compositions of arc front stratovolcanoes? Geochemistry, Geophysics, Geosystems, 16, 4178–4208. https://doi.org/10.1002/2014GC005633

Turner, S.J., Langmuir, C.H., Katz, R.F., Dungan, M.A., Escrig, S., (2016). Parental arc magma compositions dominantly controlled by mantle-wedge thermal struc-ture. Nat. Geosci.9, 772–776.

Turner, S. J., Langmuir, C. H., Dungan, M. A., & Escrig, S. (2017). The importance of mantle wedge heterogeneity to subduction zone magmatism and the origin of EM1. Earth and

Planetary Science Letters, 472, 216-228.

Trumbull, R.B., Wittenbrink, R., Hahne, K., Emmermann, R., Büsch, W., Gerstenberger, H., Siebel, W. (1999). Evidence for Late Miocene to Recent contamination of arc andesites by crustal melts in the Chilean Andes (25°–26°S) and its geodynamic implications. Journal of South American Earth Sciences 12, 135–155.

Unterschutz, J. L. E., Creaser, R. A., Thompson, R. I., & Daughtry, K. L. (2002). North American margin origin of Quesnel terrane strata in the southern Canadian Cordillera : Inferences from geochemical and Nd isotopic characteristics of Triassic metasedimentary rocks, (4), 462–475.

Varela, R., Gregori, D. A., González, P. D., & Basei, M. A. S. (2015). Caracterización geoquímica del magmatismo de arco Devónico y Carbonífero-Pérmico en el noroeste de Patagonia, Argentina. Revista de La Asociación Geológica Argentina, 72(3), 419–432.

Vergara, M., Morata, D., Hickey-Vargas, R., López-Escobar, L., & Beccar, I. (1999). Cenozoic tholeiitic volcanism in the Colbún area, Linares Precordillera, central Chile (35o35'-36oS). Revista Geológica de Chile, 26(1), 23–41.

Watt, S. F. L., Pyle, D. M., & Mather, T. A. (2011). Geology, petrology and geochemistry of the dome complex of Huequi volcano, southern Chile. Andean Geology, 38(2), 335–348.

Wood, D. A. (1980). The application of a Th-Hf-Ta diagram to problems of tectonomagmatic classification and to establishing the nature of crustal contamination of basaltic lavas of the British Tertiary Volcanic Province. Earth and Planetary Science Letters, 50(1), 11–30. https://doi.org/10.1016/0012-821X(80)90116-8

Zartman, R. E., Doe, B. R. (1981). Plumbotectonics - the Model. Tectonophysics, 75, 135–162. https://doi.org/10.1016/0040-1951(81)90213-4

Zindler, A., Hart, S. R. (1986). Chemical Geodynamics. Annual Reviews of Earth and Planetary Sciences 14: 493-571.

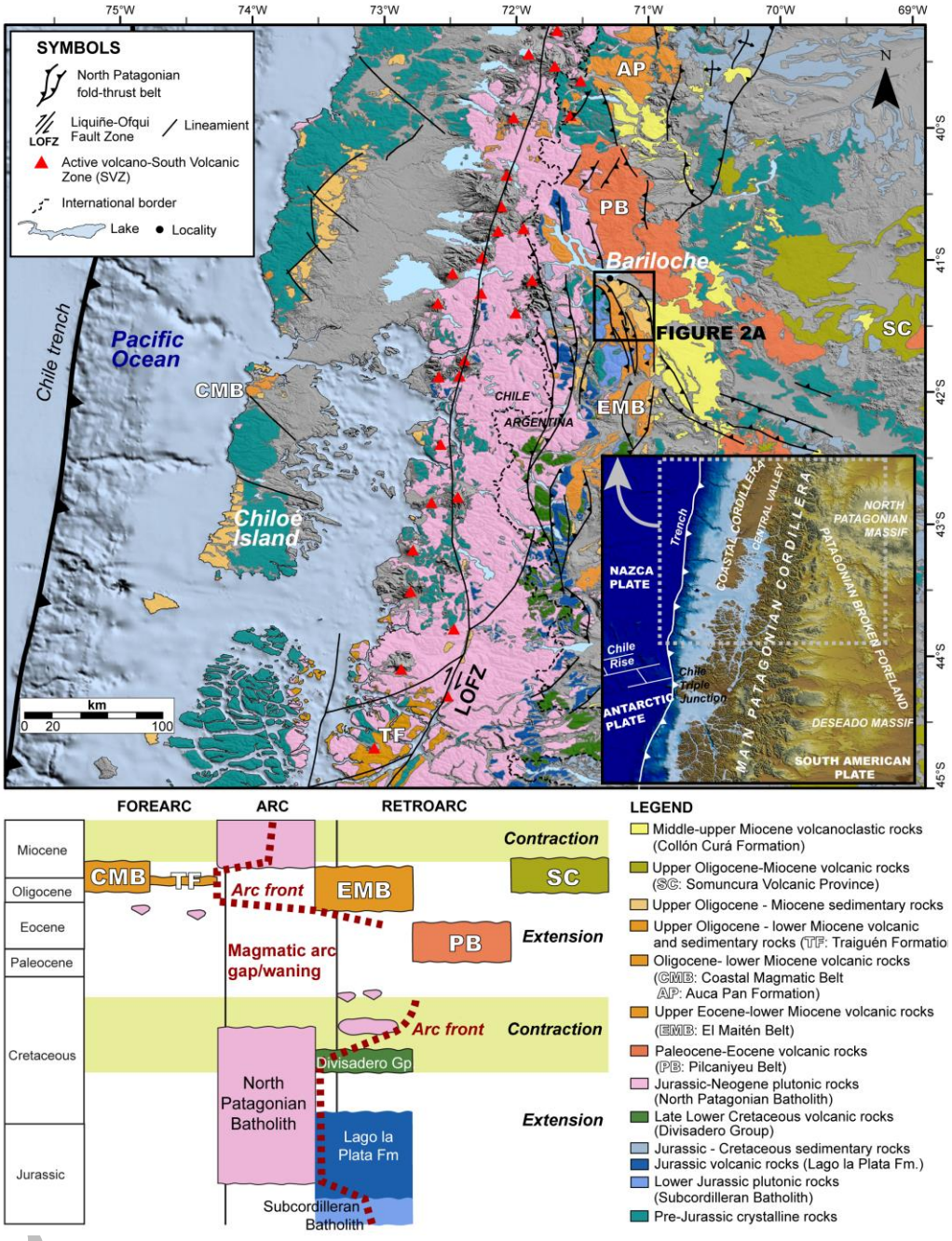

Figure 1. **a)** Regional geological map of the North Patagonian Andes and scheme of magmatic units developed during the Andean cycle. Main morphotectonic units and tectonic plates are shown in box on the lower right corner of the map. Cenozoic volcanic units include the Paleocene–middle Eocene PB=Pilcaniyeu Belt, located in the broken foreland zone; the late Eocene–lower Miocene EMB=El Maitén Belt and AP=Aucapan Formation, which crop out in the Main Patagonian Cordillera; the late Oligocene–early Miocene CMB = Costal Magmatic Belt and TF= Traiguén Formation in the Chilean area; SC= Somuncura mafic plateau developed in the foreland zone (North Patagonian Massif). LOFZ: Liquiñe-Ofqui Fault Zone. Based on Echaurren et al. (2017), González (1994), Horton (2018), Lizuain et al. (1995), and Sernageomin (2003).

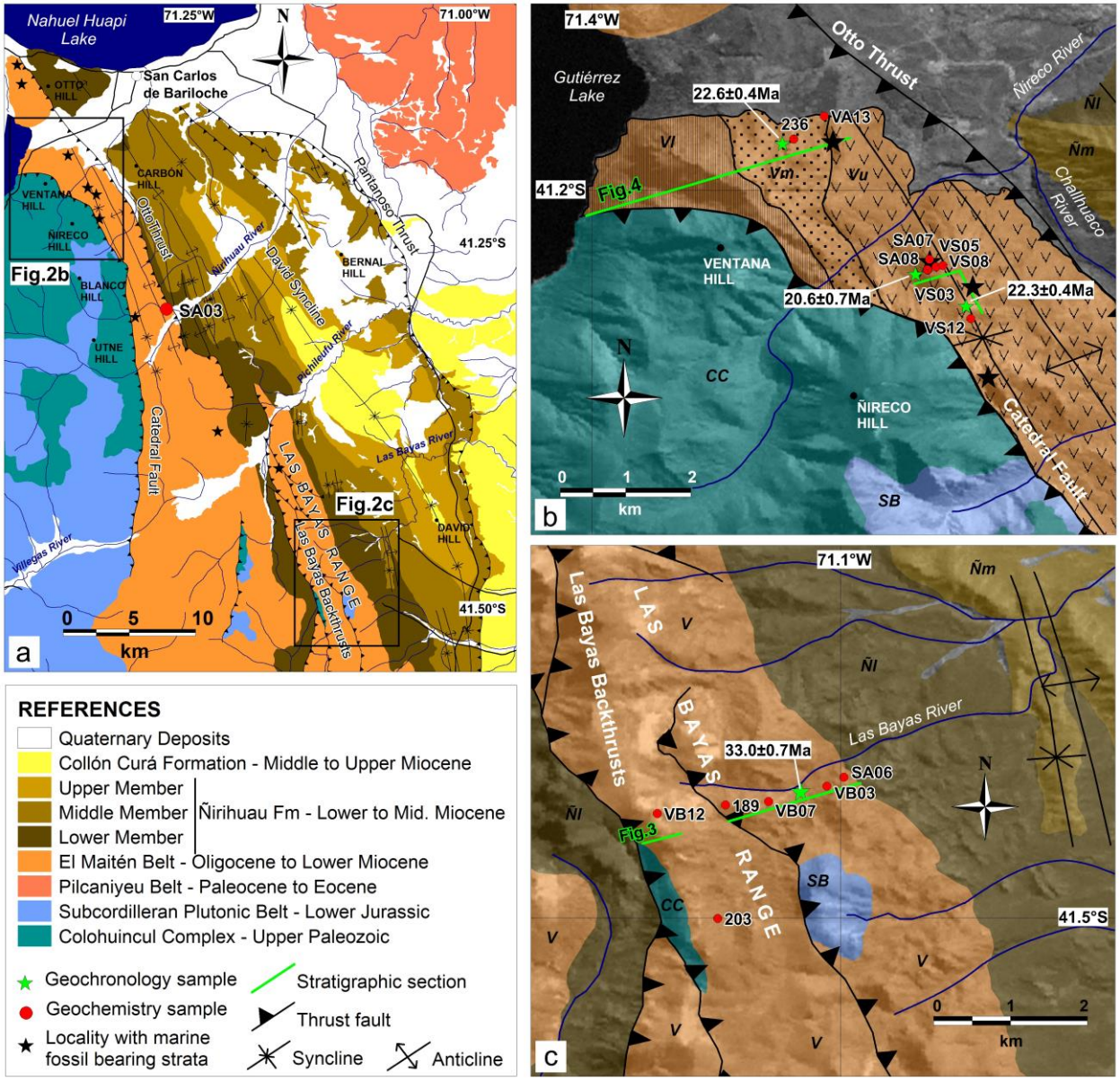

Figure 2. **a)** Geological map of the studied area, located in the northern sector of the El Maitén Belt (modified from Bechis et al., 2014). **b)** Detailed map of the Ventana and Ñireco hills area, showing the lower (Vl), middle (Vm) and upper (Vu) sections defined within the Ventana Formation stratigraphical profile; location of U-Pb data from Bechis et al. (2014) and geochemical samples are indicated. **c)** Detailed map of the Las Bayas range area; location of new U-Pb age and geochemical samples are indicated. CC: Colohuincul Complex; SB: Subcordilleran Plutonic Belt; V: Ventana Formation; Ñl: Lower member and Ñm: Middle member of Ñirihuau Formation.

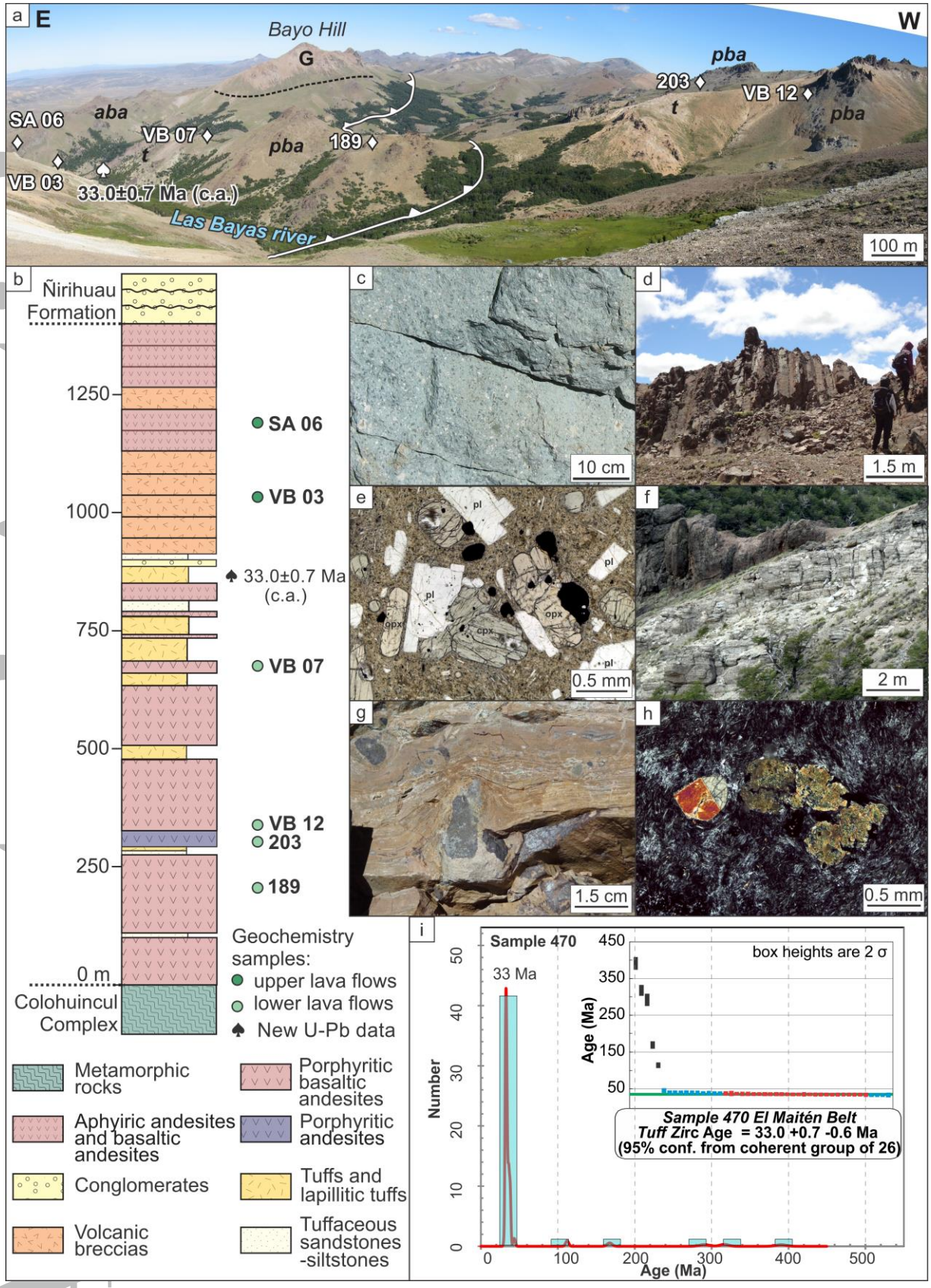

Figure 3. **a)** The El Maitén Belt sequence in Las Bayas section, showing the backthrust that repeats part of its lower and middle sections (G: granite; aba: aphanitic basaltic andesite; pba: porphyritic basaltic andesites; t: tuffs). **b)** Reconstructed stratigraphical profile of the El Maitén Belt in Las Bayas section (Fig. 2c). **c)** Porphyritic basaltic andesites from the lower

part of the section. **d)** Pyroxene-bearing basaltic andesites levels with columnar jointing. **e)** Basaltic andesite with plagioclase (pl), clinopyroxene (cpx) and orthopyroxene (opx) in a hyalopilitic groundmass. **f)** Tuffs and lapillitic tuffs from the middle part of Las Bayas section. **g)** Welded tuff from the middle part of the section. **h)** Andesite from the upper part of the section with fresh twinned clinopyroxenes and orthopyroxenes replaced by phyllosilicates, within a felty groundmass. **i)** U-Pb LA-ICP-MS zircon age from a vitreous tuff level (sample 470) from the middle part of Las Bayas section. Uncertainties are 2 sigma.

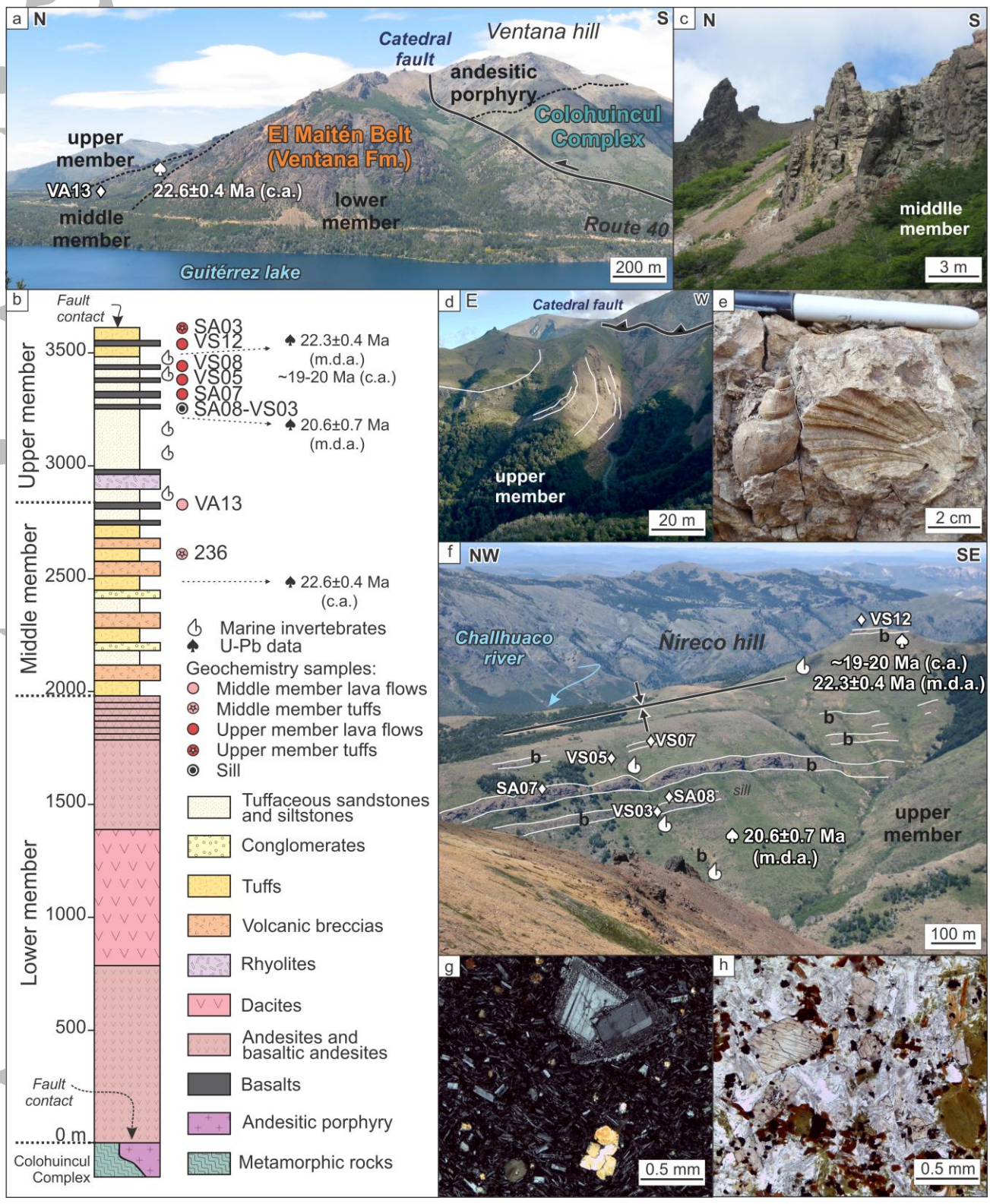

Figure 4. Ventana-Ñireco section. **a)** Lower, middle and upper sections of the Ventana Formation (Ventana hill) overlaid by the Colohuincul Complex through the Catedral fault. **b)** Stratigraphical profile of El Maitén Belt sequence (or Ventana Formation) carried out in Ventana and Ñireco hills (Fig. 2b). **c)** Pinnacles defined by sub-vertical volcanic breccias of the middle section (Ventana hill). **d)** Folded upper section in contact with the Cathedral fault (northeastern slope of the Ñireco hill). **e)** Molds of invertebrate fossils from the marine deposits interbedded at the upper section. **f)** Basaltic lava flows of the upper section (b), interbedded with marine strata (Ñireco hill). **g)** Microporphyritic basalts from the upper section, characterized by plagioclase phenocrysts with in sieve texture surrounded by an intersertal groundmass. **h)** Microporphyritic basalt from the sill that intrudes the upper section of the sequence, formed by zoned reddish clinopyroxene, replaced olivine phenocrysts, and biotite partially replaced by opaque minerals in the core. Reported ages correspond to Bechis et al. (2014). m.d.a.: maximum depositional age; c.a.: crystallization age.

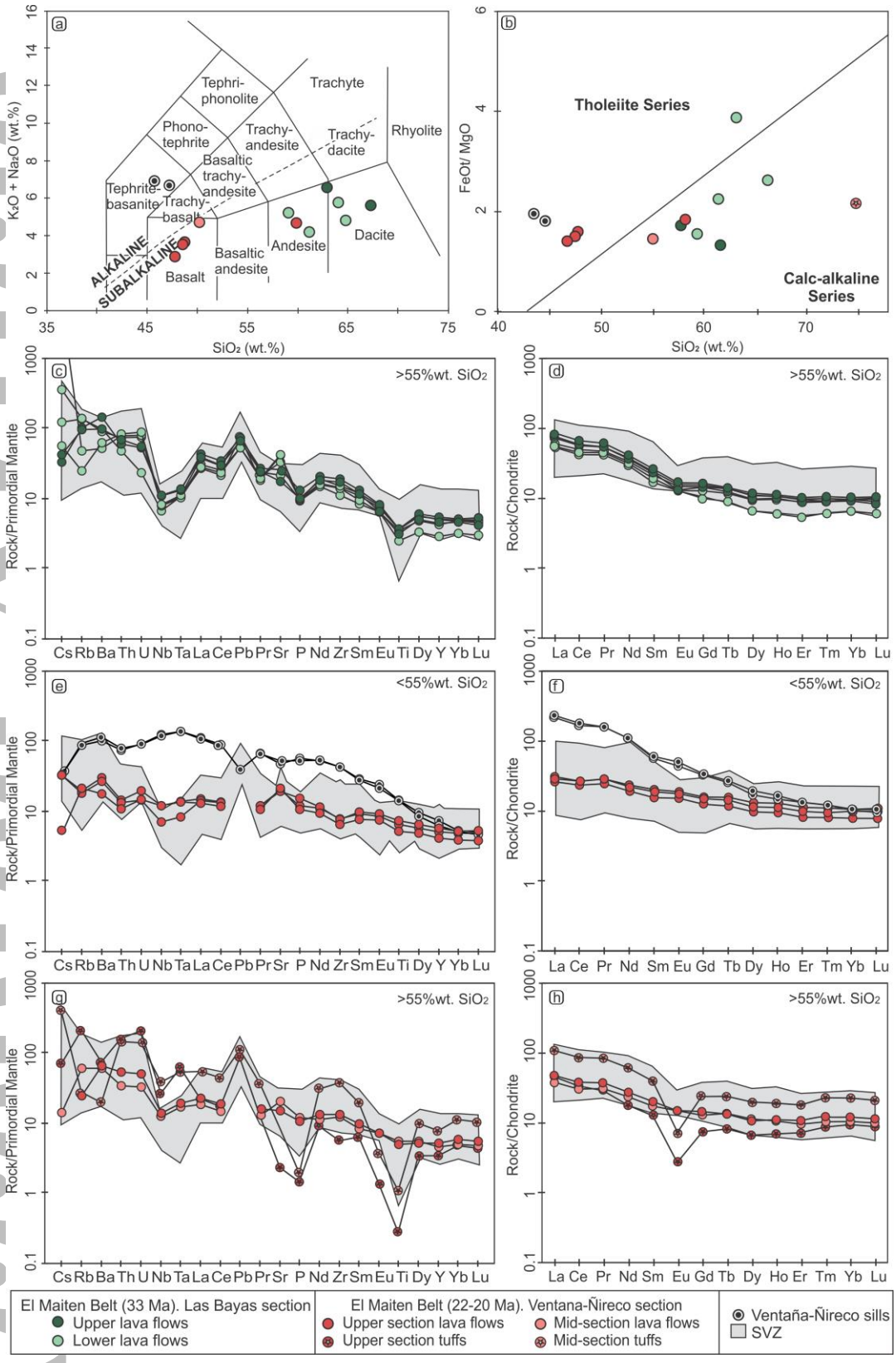

Figure 5. **a)** Total alkali versus silica classification (TAS; fields limits are according to Irvine & Baragar, 1971). The subalkaline character of the lavas from Las Bayas and Ventana-Ñireco sections contrast with the alkaline composition from the basaltic sill; the tuffs from the middle and upper members from Ventana-Ñireco plot outside silica range. **b)** FeOt/MgO versus SiO_2 (Miyashiro, 1974). Las Bayas section and the middle member of Ventana-Ñireco

section resemble calc-alkaline series, while the upper member of Ventana-Ñireco section and the basaltic sill plot within the tholeiitic field. **c-h)** Multielement plots normalized to primitive mantle values (Sun & McDonough, 1989) and chondrite-normalized (Nakamura, 1974) spider diagrams. Las Bayas samples show typical arc patterns, while Ventana-Ñireco samples show flatter patterns with less marked arc-like signature toward the upper member samples; contrastingly, the basaltic sill shows an OIB-like pattern. Samples of the SVZ are from Jacques et al. (2013), Lara et al. (2001), López-Escobar et al. (1992, 1995), Mella et al. (2005), Tobal et al. (2012), Watt et al. (2011), and references therein.

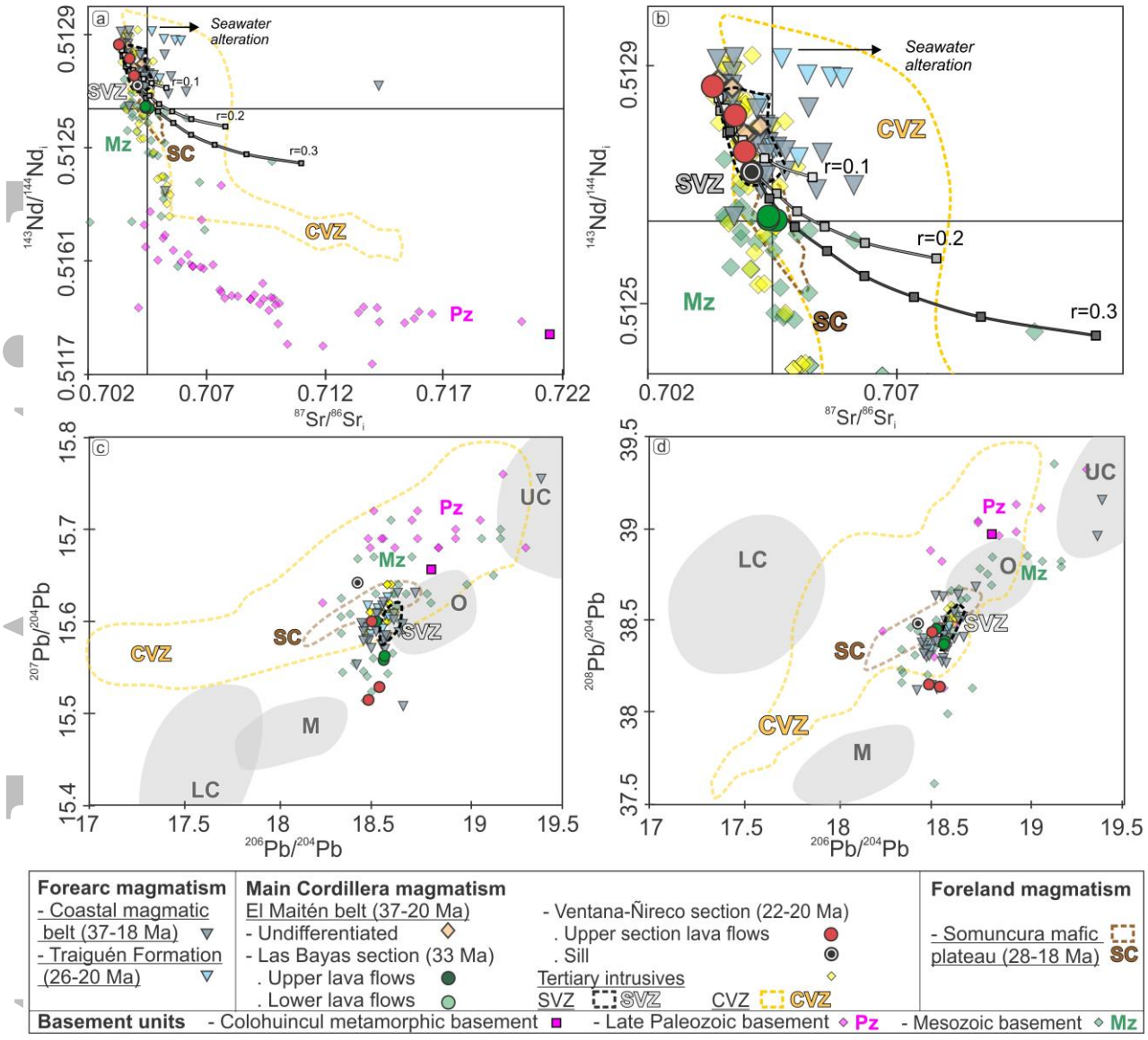

Figure 6. Isotopic composition of North Patagonian magmatism. **a and b)** $^{87}Sr/^{86}Sr_i$ versus $^{143}Nd/^{144}Ndi$ diagram and zoom to El Maitén samples, respectively. The AFC models (DePaolo, 1981) for Las Bayas samples consist of the assimilation of the Paleozoic basement (sample Pat-1B) by a parental magma with $^{87}Sr/^{86}Sri$=0,703308 and $^{143}Nd/^{144}Ndi$=0,512865 composition. In the AFC model r=Ma/Mc (rate of assimilation relative to rate of fractionation) are shown for 0.1 to 0.3; increments correspond to 10%. For details of the model see Text S5. **c)** $^{206}Pb/^{204}Pb$ versus $^{207}Pb/^{204}Pb$ diagram. **d)** $^{206}Pb/^{204}Pb$ versus $^{208}Pb/^{204}Pb$ diagram. UC: Upper Continental Crust compositions, LC: Lower Continental Crust compositions, M: Mantellic compositions, O: Orogenic compositions (Zartman & Doe, 1981). Coastal Magmatic Belt isotopic data is from Muñoz et al. (2000) and Vergara et al. (1999); Traiguén Formation from Encinas et al. (2016); undifferentiated El Maitén Belt and Somuncura mafic plateau from Kay et al. (2007); Tertiary intrusives include the Cenozoic North Patagonian Batholith and equivalents from Aragón et al. (2011a), Lucassen et al. (2004), and Pankhurst et al. (1999); the SVZ data (Southern Volcanic Zone volcanism) is from Jacques et al. (2013), López-Escobar et al. (1992, 1993, 1995) and Mella et al. (2005);

Late Paleozoic basement from Lucassen et al. (2004), Rapela et al. (2005) and Pankhurst et al. (2006); Mesozoic basement from Bouhier et al. (2017), Echaurren et al. (2017), Lucassen et al. (2004) and Rapela et al. (2005); and the CVZ (Central Volcanic Zone) from Aitcheson et al. (1995), Francis et al. (1989), Haschke et al. (2002), Lindsay et al. (2001), Rogers and Hawkesworth (1989), Ort et al. (1996), and Trumbull et al. (1999).

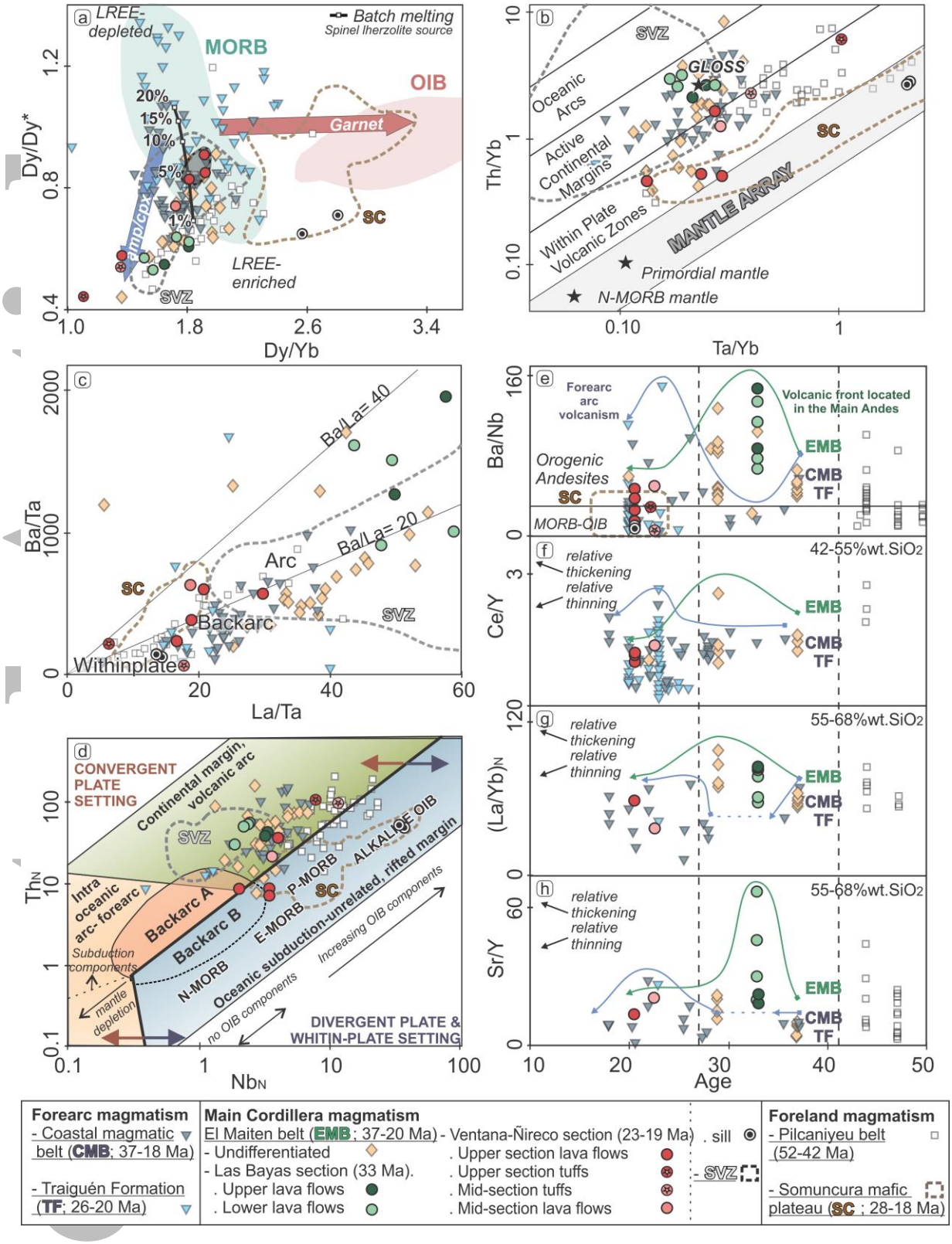

Figure 7. Geochemical tectonic discriminants for mid-Cenozoic volcanism in North Patagonia. **a)** Dy/Yb versus Dy/Dy*. Both Las Bayas and Ventana-Ñireco samples show low Dy/Yb and Dy/Dy*, assignable to cpx/amp differentiation trends (cpx=clinopyroxene and amp=amphibole stability fields) from a depleted asthenospheric (MORB) mantle source. Contrastingly, the samples of the sill show high Dy/Yb ratios that indicate higher pressures at the mantle melting site (GAR=garnet stability field), typical of OIB sources. Result of the

batch melting model are included, indicating that Ventana-Ñireco basalts potentially match with about 5% of melting of a spinel lherzolite. **b)** Th/Yb versus Ta/Yb (Gorton & Schandl, 2000; Pearce, 1983). Higher Th/Yb ratios indicative of Active Continental margin settings discriminate Las Bayas samples from the lower Th/Yb ratios of the Ventana Ñireco samples, whereas the higher Th/Ta ratios of the sill correspond to the Mantle Array field. **c)** Ba/Ta versus La/Ta. Higher Ba/Ta ratios of Las Bayas samples indicate an arc setting, in contrast with Ventana-Ñireco samples that plot in the backarc field and the samples of the sill that plot closer to withinplate values. **d)** Th_N versus Nb_N (Saccani, 2015), normalized to the N-MORB composition (Sun & McDonough, 1989). The thick black line separates Convergent Plate Settings, characterized by brown and green shades, from Divergent Plate Settings in shades of blue. Las Bayas samples show Th_N and Nb_N values in the range of continental volcanic arcs, whereas the trend of Ventana-Ñireco samples toward lower Th_N, is more frequent in Divergent Plate Settings; the sill plot in the OIB alkaline field. **e, f, g and h)** Ba/Nb, Ce/Y, La/Yb_N (normalized to chondritic values: McDonough & Sun, 1995) and Sr/Y respectively versus age. Ba/Nb is used as a measure of slab contributions, while Ce/Y, La/Yb_N and Sr/Y represent proxies for crustal thickness. These diagrams are focused on arc-related rocks, so the samples of the sill were not included. Green arrows indicate El Maitén Belt evolution over time (EMB), while blue arrows show forearc evolution including the Coastal Magmatic Belt and the Traiguén Formation samples (CMB; TF). Samples of CMB are from Henríquez Ascencio (2016), López-Escobar & Vergara (1997), and Muñoz et al. (2000); samples of the TF from Encinas et al. (2016), Henríquez Ascencio (2016), and Hervé et al. (1995); samples of undifferentiated EMB from Aragón et al. (2011a), Iannelli et al. (2017) and Kay et al. (2007a); samples of the SVZ from Jacques et al. (2013), Lara et al. (2001), López-Escobar et al. (1992, 1995), Mella et al. (2005), Tobal et al. (2012), Watt et al. (2011), and references therein; samples from Pilcaniyeu Belt from Aragón et al. (2011b) and Iannelli et al. (2017); and samples from Somuncura mafic plateau (SC) from Asiain et al. (2017) and Kay et al. (2007).

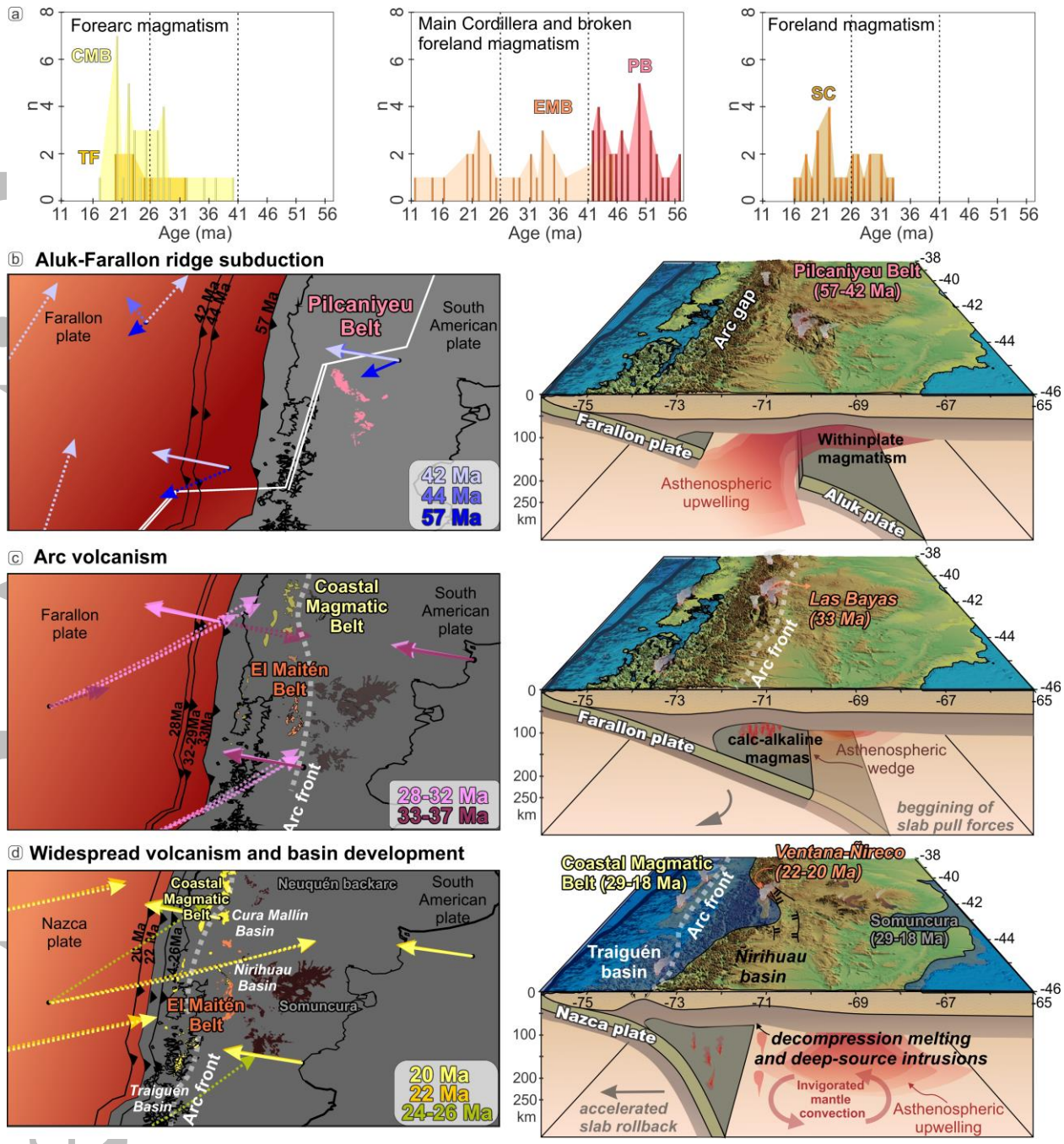

Figure 8. **a)** Age distribution of studied volcanic sequences. TF=Traiguén Formation; CMB=Coastal Magmatic Belt, EMB=El Maitén Belt; PB=Pilcaniyeu Belt; SC=Somuncura mafic magmatism. **b, c, and d)** Tectonic model for the evolution of Paleocene–early Miocene North Patagonian magmatism, which includes Paleocene ridge subduction (based on Aragón et al., 2013), late Eocene–Oligocene arc consolidation, and late Oligocene–early Miocene widespread extension during Nazca Plate rollback, respectively. The left column shows paleogeographic distribution of magmatic units, trench positions and arrows representing angle of convergence and plate velocities (Matthews et al., 2016). Dotted arrows represent Farallon/Nazca oceanic plate velocities, while filled arrows show South American plate velocity. Ages of magmatic units are from Aragón et al., (2011 a, b), Ardolino & Franchi, (1993); Bechis et al., (2014), Benedini et al., (2017), Coira et al., (1985), Corbella et al. (1982 a, b), Encinas et al., (2016), Fernández Paz et al., (2018), González Díaz, (1979), Henríquez Ascencio, (2016), Hervé et al., (1995), Iannelli et al., (2017), Kay et al., (2007), Lizuain &

Viera, (2010), Marshall et al., (1983, 1986); Mazzoni et al., (1991), Muñoz et al., (2000), Ramos et al., (2014), Rapela et al., (1983, 1988), Remesal et al., (2012), and Turner, (1982). The right column comprises the tectonic schemes for the different stages of North Patagonian Andes evolution.